Decarbonizing ethanol production via gas fermentation
Impact of the $CO/H_2/CO_2$ mix source on greenhouse gas emissions and production costs

Almeida Benalcázar, Eduardo; Noorman, Henk; Maciel Filho, Rubens; Posada, John A.

DOI
10.1016/j.compchemeng.2022.107670

Publication date
2022

Document Version
Final published version

Published in
Computers and Chemical Engineering

Computers and Chemical Engineering 159 (2022) 107670

Contents lists available at ScienceDirect

Computers and Chemical Engineering

journal homepage: www.elsevier.com/locate/compchemeng

Decarbonizing ethanol production via gas fermentation: Impact of the $CO/H_2/CO_2$ mix source on greenhouse gas emissions and production costs

Eduardo Almeida Benalcázar[a,b,*], Henk Noorman[b,c], Rubens Maciel Filho[a], John A. Posada[b]

[a] Department of Product and Process Development, Faculty of Chemical Engineering, State University of Campinas, Av. Albert Einstein 500, Campinas, SP 13083-852, Brazil
[b] Department of Biotechnology, Faculty of Applied Sciences, Delft University of Technology, Van der Maasweg 9, Delft 2629 HZ, the Netherland
[c] DSM Biotechnology Center, A. Fleminglaan 1, Delft 2613 AX, the Netherland

ARTICLE INFO

Article history:
Received 14 December 2020
Revised 17 August 2021
Accepted 2 January 2022
Available online 15 January 2022

Keywords:
Gas fermentation
Ethanol
Process optimization
Sensitivity analysis
Bubble column
Syngas

ABSTRACT

This study explores key success factors for ethanol production via fermentation of gas streams, by assessing the effects of eight process variables driving the fermentation performance on the production costs and greenhouse gas emissions. Three fermentation feedstocks are assessed: off-gases from the steel industry, lignocellulosic biomass-derived syngas and a mixture of H_2 and CO_2. The analysis is done through a sequence of (i) sensitivity analyses based on stochastic simulations and (ii) multi-objective optimizations. In economic terms, the use of steel off-gas leads to the best performance and the highest robustness to low mass transfer coefficients, low microbial tolerance to ethanol, acetic-acid co-production and to dilution of the gas feed with CO_2, due to the relatively high temperature at which the gas feedstock is available. The ethanol produced from the three feedstocks lead to lower greenhouse gas emissions than fossil-based gasoline and compete with first and second generation ethanol.

1. Introduction

Global policy efforts aiming to reduce the anthropogenic emissions of greenhouse gases (GHG) and to guarantee the security of energy supply converge into the need for progressive replacement of fossil-based fuels by low-carbon and renewable fuels (COP-UNFCCC, 2016; Edenhofer et al., 2014), such as ethanol. The use of sugarcane juice and corn as feedstocks for large-scale production of ethanol is currently a mature and widespread technology that achieves significant reductions on GHG emissions compared to fossil-based gasoline and diesel (Edenhofer et al., 2014). However, there are concerns about the (direct and indirect) land use change and potential conflicts with animal and human food supply derived from these feedstocks (Bitnere and Searle, 2017; European Parliament, 2018). In response, the use of gaseous feedstocks has gained attention from academia and industry in recent years (Achinas et al., 2019; Liew et al., 2016; Phillips et al., 2017).

Syngas is a gas mixture of CO, CO_2 and H_2 that can be produced from the thermochemical conversion of lignocellulosic biomass, municipal solid wastes or other industrial organic wastes (Liew et al., 2016), and also via reforming of methane (Teixeira et al., 2018). Syngas can be used for the production of bulk chemicals and fuels through fermentation (Almeida Benalcázar et al., 2017; Sun et al., 2019). Such process exploits the ability of acetogenic bacteria to retrieve the energy contained in CO and H_2 while fixing the carbon from CO and CO_2. The main native products of these types of microorganisms are formic, acetic and lactic acids, ethanol and 2,3-butanediol (Bertsch and Müller, 2015; Liew et al., 2016; Oswald et al., 2018; Ragsdale and Pierce, 2008). In addition, since acetogens are able to catabolize the components of syngas in a wide range of compositions (Abubackar et al., 2015; Leang et al., 2013), industry and academia have contemplated other sources of fermentable CO, H_2 and CO_2 *e.g.*, industrial off-gases from steel manufacturing (Simpson et al., 2012) and gas mixtures containing H_2 derived from the electrolysis of water (Simpson et al., 2017) and CO_2 derived from the combustion of carbonaceous materials.

The diversity of laboratory and pilot-plant set-ups for ethanol production through gas fermentations is wide as they include different microbial strains (*e.g.*, mesophilic and thermophilic bac-

* Corresponding author at: Department of Biotechnology, Faculty of Applied Sciences, Delft University of Technology, Van der Maasweg 9, Delft 2629 HZ, the Netherland.
E-mail address: e.f.almeidabenalcazar@tudelft.nl (E. Almeida Benalcázar).

https://doi.org/10.1016/j.compchemeng.2022.107670

Glossary

BBS	bio-based syngas
BOF	basic oxygen furnace
CAC	CO_2 abatement costs
C	concentration in fermentation broth
C^*	saturation concentration
F	molar flow rate
f_{Dil}	syngas dilution factor
f_{k_La}	mass transfer coefficient factor
f_{Ac^-}	acetic acid co-production factor
FDC	facility-dependent costs
GHG	greenhouse gases
GWP	global warming potential
h_L	height of the liquid column
IV	model input variable
k_H	Henry's coefficient
k_La	gas-liquid mass transfer coefficient
OV	model output variable
p	absolute pressure
q	biomass specific production/consumption rate
R	volumetric productivity
T	fermentation temperature
U_S	gas utilization
$\dot{V}$	volumetric flow rate
v^c_{sG}	pressure corrected superficial gas velocity
y	molar fraction in gas phase
$Y_{x/CS}$	biomass yield
$\Delta G'$	free Gibbs energy change at physiological conditions

Subscripts

cat	catabolic
D	electron donor of catabolism *i.e.* CO, H_2
et	ethanol
G	gas
i	entering to the syngas fermentor
L	fermentation broth
lm	logarithmic mean
o	exiting the syngas fermentor
S	syngas components *i.e.* CO, H_2, CO_2
x	dry microbial biomass

Superscripts

max	maximum
met	metabolic

teria) (Martin et al., 2016), batch and continuous operations (Kundiyana et al., 2010; Valgepea et al., 2018), fermentation in single and multiple stages (Richter et al., 2013; Trevethick et al., 2017), thermophilic (Daniel et al., 1990; Sakai et al., 2004) and high pressure operation (Oswald et al., 2018), plus the use of an assortment of internals (monoliths, membranes, external recycles, among others) as part of the bioreactors (Asimakopoulos et al., 2018; Bredwell et al., 1999; Kim and Lee, 2016; Li, 2016; Shen et al., 2017, 2014a, 2014b; Yasin et al., 2015). This variety altogether converges into the search of overcoming the low solvent productivity, which is commonly credited to the poor solubility of CO and H_2 in the fermentation broth. From an analysis of the published literature on gas fermentation it is clear that, although the limitation of low productivity has been addressed during the past two decades, it is uncertain what other variables controlling the fermentation may benefit the development and scale-up of the process.

It has been advocated that the design of experiments at laboratory scale aimed at the development of industrial-scale fermentation processes must be guided by "the perspective of the large-scale" (Noorman, 2011). For this purpose, the only publicly available report based on corporate data is an environmental sustainability assessment for the production of ethanol from the fermentation of steel manufacturing off-gases (Handler et al., 2016), which concluded that the global warming potential (GWP) of such process equals 31 g_{CO2e}/MJ of ethanol. To put this number into perspective, one can consider that ethanol's net standard enthalpy of combustion is 26.8 MJ/kg (Perry and Green, 2003) and that at full combustion 1 kg of the alcohol will release 1913 g of CO_2, thus the production of the biofuel should not generate more than 71.3 g_{CO2e}/MJ of ethanol. In the same study (Handler et al., 2016), unrevealed data from the bioreactor performance is also used to estimate the GWP of ethanol produced from biomass-derived syngas in the range of 2–12 g_{CO2e}/MJ. Moreover, research efforts have been made to understand the linkage between the syngas fermentation conditions (in combination with the up and downstream processes) and the techno-economic and environmental performances of different process configurations. Such studies use Aspen Plus to simulate the bioreactor, with simplified models and their simulations offer little detail about the operation of the bioreactor; a unit with still large development challenges ahead. Another study, was devoted to gaining insights on variables that may optimize the economic and environmental performance of the bioreactor and the downstream processing of ethanol (de Medeiros et al., 2020); however, that study left the production of the syngas feedstock out of the battery limits, disregarding the large potential for heat integration offered by the hot gas stream.

As a starting point, we developed a black-box model of bacteria to simulate ethanol production in a 700 m^3 bubble column bioreactor fed by CO, H_2 and CO_2 mixtures (Almeida Benalcázar et al., 2020a). Then a stochastic bioreactor simulation using the same model suggested that ethanol volumetric productivity and gas utilization have a 50% probability of reaching values between 2.5–6.8 g/L/h and 30 – 66%, respectively (Almeida Benalcázar et al., 2020b). However, it is unclear whether such indicators will render, the overall ethanol production process, economically and environmentally attractive, and to what extent the potential for commercial success would depend on the selection of a gas stream source with a specific composition. Thus, this study seeks to identify key parameters and their combinations that may drive the fermentation process to simultaneously achieve minimal ethanol production costs and GHG emissions. The assessment is applied to three process configurations which primarily differ in the gas source and its production process to provide gas mixtures of different compositions. Finally, the assessment also seeks to: (*i*) determine the potential of such process configurations to constitute viable options to replace fossil-based fuels and other bio-based ethanol production routes (*e.g.* 1G and 2G ethanol) at a competitive cost in the medium term, and (*ii*) provide direction for future research efforts on design and integration of the fermentation stage with the up and downstream operations.

2. Methodology

This section details the sequence of steps followed to assess the robustness and to simultaneously minimize the economic performance and environmental impacts of ethanol production from three different gas mixtures containing CO, H_2 and CO_2. Both, the sensitivity analyses and the optimizations are performed by varying eight process variables that command the operation of the fermentation process, namely: (*i*) process temperature (T), (*ii*) top reactor pressure (p_t), (*iii*) gas feed dilution (f_{Dil}), (*iv*) maximum ethanol concentration (C^{max}_{et}), (*v*) liquid column height (h_L), (*vi*) mass transfer coefficient factor (f_{k_La}), (*vii*) acetic acid production factor (f_{Ac^-}) and (*viii*) the pressure-corrected superficial gas velocity (v^c_{sG}). These eight variables are referred to as input variables

(*IV*'s), while the indicators used to quantify the overall economic performance and environmental impacts of the ethanol production process are called output variables (*OV*'s). The following sections describe how the *IV*'s are processed in order to obtain the *OV*'s.

2.1. Process configurations

Three process configurations are analyzed in this study; they differ primarily on the gas source, meaning different compositions and production processes. The selection of the gas source is based on three major aspects: (*i*) the gas compositions should range between pure CO and a mixture of H_2/CO_2, (*ii*) there must be reports showing academic and industrial interest in the specific gas mixture, and (*iii*) the environmental impacts at the gas production stage should be diverse among the choices. Thus, the considered gas feedstocks are:

- CO-rich basic oxygen furnace (from here referred to as BOF) off-gas from the steel manufacturing process (Handler et al., 2016).
- A 3:1 mixture of H_2 and CO_2 (from here referred to as HAC), where H_2 is derived from water electrolysis, and CO_2 scrubbed from a generic industrial combustion flue-gas (Simpson et al., 2017; Teixeira et al., 2018). The 3:1 mixture comes from the stoichiometric relation between the two gases for producing ethanol at the fermentation.
- Bio-based syngas (from here referred to as BBS) with a H_2/CO ratio of 2 and produced by gasification of lignocellulosic biomass (Almeida Benalcázar et al., 2017).

All process configurations have a fixed ethanol throughput of 220 kton/y, a scale that may be regarded as conservative, considering that the National Renewable Energy Laboratory bases its popular conceptual second-generation ethanol designs on a 2000 ton/d (660 kton/y assuming a year of 330 operative days) capacity in the United States (Davis et al., 2015).

As shown in Table 1, the BOF off-gas (or converter gas) is generated at a temperature of 1100 °C and at ambient pressure (NEDO, 2008; Remus, 2013); the BOF off-gas is then conditioned to remove main impurities, cooled and compressed before entering to the fermentation (Handler et al., 2016). In the H_2/CO_2 mixture, H_2 is produced at 70 °C and a pressure of 10 bar (Harrison et al., 2009; Rey Porto et al., 2010), while CO_2 is obtained pure and compressed after scrubbing it from a flue-gas stream using monoethanolamine (Husebye et al., 2012); no conditioning is required for this gas mixture prior entering to the fermentation. Finally, the BBS is produced at 900 °C and ambient pressure; the gas is then conditioned and cooled before entering the fermentation (Almeida Benalcázar et al., 2017).

The fermentation process consists of a 700 m^3 bubble column fermentor (a common volume in industry (Shaikh and Al-Dahhan, 2013)) fed by the gas mixture (see Fig. 1). The ethanol produced inside the fermentor exits through two routes: (*i*) along the liquid fermentation broth outflow, and (*ii*) pre-concentrated along the off-gas (from where it is subsequently condensed and recovered by flash separation). The alcohol is separated from the two streams by atmospheric distillation and purified with a molecular sieve. The acetic acid and the cells produced in the fermentation are directed to wastewater treatment where they are converted into biogas which is subsequently combusted for heat integration (see Section 2.2.3).

In the cases of BOF off-gas and BBS fermentations, the unconsumed gas is treated as a waste and combusted before being released into the atmosphere, as proposed by Handler et al. (2016). For HAC instead, the unconsumed gas is recycled to the fermentation to avoid waste of the expensive gases. Gas recycling would not be feasible for the BOF off-gas and the BBS fermentations because the gas feedstocks have impurities (mainly CH_4 and N_2 Ciferno and Marano, 2002) that may accumulate if the bioreactor off-gas was recycled.

Table 1
Compositions, temperature and pressure at which the three gas feedstocks are available.

Gas source	Composition[a] (%)			Temperature (°C)	Absolute pressure (atm.)
	CO	CO_2	H_2		
BOF	55–100	0–45	0	1100	1
HAC	0	25–58.7	41.3–75	70	10
BBS	18.3–33.3	16.7–54.2	27.5–50	900	1

[a] The ranges of compositions have been approximated from literature reports for BOF off-gas (Bieda, 2012) and BBS (Almeida Benalcázar et al., 2017; Dutta et al., 2011). CO_2 content in BBS is higher from what is commonly reported in literature as here, extra CO_2 was used for simulating the effect of the dilution of syngas with any inert component.

2.2. Strategy for process simulation

Mass and energy balances at the fermentation stage allow integration with ethanol downstream processing and the upstream gas production processes. The fermentation stage comprises the unit operations directly linked to the fermentation *i.e.*, the bioreactor (R in Fig. 1), the inlet and outlet gas compressors (C1 and C2 in Fig. 1) plus the condenser and the flash separation drum (N and F in Fig. 1, respectively). Since more than 50% of the ethanol production costs and environmental impacts may be derived from the operations constituting the fermentation stage (Almeida Benalcázar et al., 2017), the model for the fermentation is the most detailed of all unit operations in the three process configurations; the simulations of the bioreactors are described below.

2.2.1. Simulation of the bioreactor for the BOF and the HAC fermentations

The bioreactor model used in this study has been presented, thoroughly described and partially validated elsewhere (Almeida Benalcázar et al., 2020a); therefore only the model's basic structure is detailed in this section. The consumption of CO and H_2 are simulated independently since the applied black-box model of microbial reactions is not able to consider the uptake of more than one electron donor at a time. The method for simulating the fermentation of syngas which contains both electron donors, CO and H_2, is introduced in Section 2.2.2.

The fermentation model interlinks a thermodynamics-based black-box model of main microbial reactions and a mass transfer-based model of a large-scale bubble column bioreactor. In the black-box model, a simplified reaction is constructed to describe the microbial metabolism from the combination of catabolic (see Eqs. (1)–(4) in Table 2) and anabolic reactions (see Eqs. (5) and (6)). Ethanol and acetic acid are assumed the two only possible products of catabolism which harnesses the chemical energy contained in the electron donors. Other products, such as formic acid or 2,3-butanediol (Oswald et al., 2018; Valgepea et al., 2018) are not considered in this study because the drivers favoring their selectivity by bacteria are not clearly understood and also because the effect of a reduction on the ethanol yield is already simulated by the co-production of acetic acid. The black-box model is built such that the kinetic and stoichiometric parameters are dependent on the process temperature and the intracellular concentrations of CO, H_2, CO_2, ethanol, acetic acid and H^+ ions. Since CO, H_2, CO_2 and ethanol diffuse freely across the bacterial membrane, their intracellular concentrations are assumed equal to the extracellular ones. The intracellular concentration of H^+ ions is assumed constant at 1×10^{-7} M (neutral pH) whereas the intracellu-

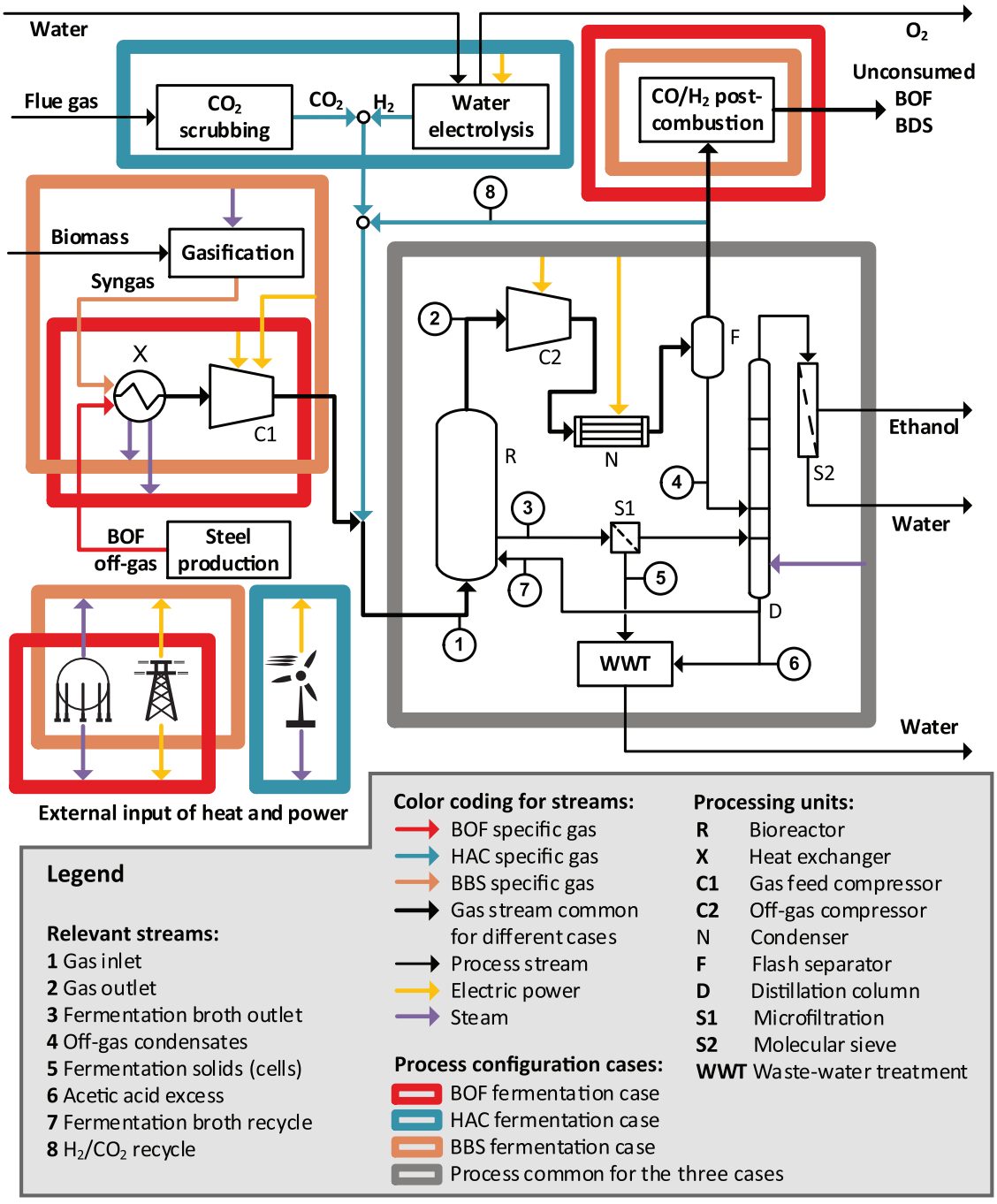

Fig. 1. Configurations of the ethanol production processes depending on gas production. The units concealed inside the colored battery limits are the units included in the economic and environmental assessments.

Table 2
Catabolic and anabolic reactions considered by the black-box model of microbial reactions.

Phase of metabolism	Reaction	Equation nr.
Catabolism	$6CO + 3H_2O \rightarrow C_2H_5OH + 4CO_2$	(1)
	$6H_2 + 2CO_2 \rightarrow C_2H_5OH + 3H_2O$	(2)
	$4CO + 2H_2O \rightarrow CH_3COO^- + H^+ + 2CO_2$	(3)
	$4H_2 + 2CO_2 \rightarrow CH_3COO^- + H^+ + 2H_2O$	(4)
Anabolism	$2CO + \frac{1}{4}NH_4^+ + \frac{1}{2}H_2O \rightarrow CH_{1.75}O_{0.5}N_{0.25} + CO_2 + \frac{1}{4}H^+$	(5)
	$2H_2 + CO_2 + \frac{1}{4}NH_4^+ \rightarrow CH_{1.75}O_{0.5}N_{0.25} + \frac{3}{2}H_2O + \frac{1}{4}H^+$	(6)

lar concentration of acetate ions is electrochemically dependent on the extracellular pH and the concentration of acetate (van Maris et al., 2004). Since it is unknown whether the acetate ions will be at equilibrium at both sides of the bacterial membrane, the intracellular concentration of acetate is assumed to be 100 mM (Mock et al., 2015) while the extracellular pH and the total concentrations of acetate plus acetic acid are assumed constant at 4.5 and 142.5 mM (Richter et al., 2013).

The equations used by the black-box model to estimate the thermodynamic feasibility of catabolism (when the Gibbs free energy change, $\Delta G^{T'}_{cat,D}$ < -9 kJ/mol Müller and Hess, 2017), as well as the stoichiometric and kinetic parameters of the microbial reactions are shown in Table SI1 in the Supplementary Information (SI).

Furthermore, it is assumed that the bioreactor operates in continuous mode at steady-state. In the bioreactor, gas-to-liquid mass transfer is driven by the energy input provided by gas sparging and the dissolved gas concentration gradients (Heijnen and Van't Riet, 1984; Van't Riet and Tramper, 1991). Thus, mass transfer coefficients ($k_L a_S$) are estimated as function of the v^c_{sG}. The saturation concentrations of the gas components (C^*_S) are estimated using Henry's equation; the temperature-dependent Henry's coefficients are gathered from Sander (2015). The specific equations used by the mass transfer model are shown in Table SI2 at the SI.

Since both, the black-box model of microbial reactions and the mass transfer model, depend on the dissolved concentration of the gas components (C_S), the operation of the bioreactor is evaluated at 200 different values of the mean-log dissolved concentration of the electron donor (C_D) [1] *i.e.*, CO for BOF, and H_2 for HAC fermentations, respectively. The values of C_D are set to range between the saturation concentration and their thermodynamic thresholds (where $\Delta G^{T'}_{cat,D}$ = -9 kJ/mol). The system of equations formed by the mass balances is fully specified and has multiple solutions. Therefore, an ethanol productivity optimization function is used to determine operation points of the bioreactor at each value of C_D. For further details on this optimization, the reader is referred to Almeida Benalcázar et al. (2020a). The reader is also advised that this optimization is not yet the multi-objective process optimization, which will be explained in Section 2.5.

From the whole range of 200 possible bioreactor operation points, one is selected to characterize the bioreactor operation at a defined combination of input variables (*IV*'s). Such point must fulfill five conditions to assume that the fermentation process operates at an optimal state that is comparable to a bioreactor operating with a different set of *IV*'s: (*i*) mass transfer rate exceeds the 90% of its maximum (evaluated at the CO and H_2 thresholds); (*ii*) electron donors do not fall below threshold concentrations at the top of the liquid column; (*iii*) CO concentration does not exceed 0.06 mM at the bottom of the column, so CO uptake inhibition (Li et al., 2017; Mohammadi et al., 2014) could be evaded; (*iv*) the biomass production rate is low enough such that the liquid outflow rate ($\dot{V}_{L,o}$) from the bioreactor does not prevent ethanol from achieving C^{max}_{et}; and (*v*) the biomass concentration in the bioreactor does not surpass 10 g/L (Richter et al., 2013). When several points fulfill these conditions, the one with the highest ethanol volumetric productivity is selected.

Fig. 2 shows a schematic representation of the connections between the model *IV*'s (light pink blocks in Fig. 2) and *OV*'s (light orange in Fig. 2). The *IV*'s T, p_t, h_L and v^c_{sG} are directly set into the model. In turn, the f_{Dil} is conceived as a consequence of the gas-supply process configurations and is included in the algorithm by adding an excess of CO_2 into the gas feed. Stoichiometrically, any CO_2 present in BOF off-gas or in BBS (with a H_2/CO ratio of 2) is considered an excess and therefore 'dilution' (considering the ratios of CO, H_2 and CO_2 needed for the catabolic production of ethanol from CO - Eq. (1) and from H_2 and CO – Eq. (7)). Moreover, the *IV* C^{max}_{et} is introduced in the ethanol productivity optimization as an upper boundary to constrain the ethanol concentration solutions (Almeida Benalcázar et al., 2020a). Lastly, the ratio between the biomass-specific acetate production rate and the total rate of product generation (*IV* f_{Ac^-}), which determines how much acetate is produced along ethanol, is introduced in the model as a factor defined by Eq. (8) Solving the system of mass and energy balances is more stable when the loop uses the solutions of an adjacent point as initial guesses. The 200 points gives a leveled balance between resolution and processing speed.

$$6H_2 + 2CO \rightarrow C_2H_5OH + 3H_2O \tag{7}$$

$$f_{Ac^-} = \frac{q_{Ac^-}}{q_{Ac^-} + q_{et}} \tag{8}$$

The C_D profiles along the height of the liquid column, inside the bioreactor, are estimated by discretizing the height of the column into a number of equal parts that are determined following the methodology recommended in Almeida Benalcázar et al. (2020a). Mass balances are solved for each portion of the column assuming that concentration of cells and ethanol are homogeneous and that the gas phase behaves as a plug-flow.

2.2.2. Simulation of the bioreactor for BBS fermentation

Since the black-box model of microbial reactions is only able to simulate the consumption of one electron donor at a time, the fermentation of bio-based syngas, which contains two electron donors, CO and H_2, is simulated indirectly. Each *k*th mass and energy stream (MES) going in and out the BBS fermentation stage is estimated by adding the contributions of the independent fermentations that use pure CO and the 3:1 H_2/CO_2 mixture, at their respective operation points. Such fractional contributions (contained within parentheses in Eq. (9)) are determined by the H_2/CO ratio (*HC*) in the BBS fermentor.

$$MES_{k,BDS} = MES_{k,CO}\left(\frac{1}{1+HC}\right) + MES_{k,H_2/CO_2}\left(\frac{HC}{1+HC}\right) \tag{9}$$

A thorough description of the streams considered for the mass and energy balances is included in Tables SI2 and SI3 in the SI.

2.2.3. Sources of energy and heat integration

The energy requirements of the fermentation stage plus the ethanol downstream processing consider: (*i*) the electric energy required by the inlet and outlet gas compressors, (*ii*) the electric energy needed by the cryogenic condensation (at -6 °C) of ethanol and water stripped from the bioreactor by the off-gas, and (*iii*) the steam needed by the distillation. The energy needed by the unit operations that use cooling water as utility (*i.e.* the bioreactor, and the off-gas cooling prior to the condensation) is not included in the energy accounting because it is negligible (Almeida Benalcázar et al., 2017).

The BOF off-gas and the BBS streams are available at high temperatures (see Table 1) and they are cooled before entering the fermentation (unit X in Fig. 1). Thus the sensible heat from the cooling operation is recovered to produce steam (see violet arrows leaving unit X in Fig. 1) with an energetic efficiency of 85% (Handler et al., 2016). The produced steam is used at the ethanol distillation in the BOF case and in biomass gasification in the BBS case; for the scenarios in the stochastic simulation in which the steam produced by heat integration does not cover the needs of the distillation and the gasification, additional steam is produced as a utility; on the other hand, an excess of steam produced by the heat integration will not bring any benefits because although

[1] Solving the system of mass and energy balances is more stable when the loop uses the solutions of an adjacent point as initial guesses. The 200 points gives a leveled balance between resolution and processing speed.

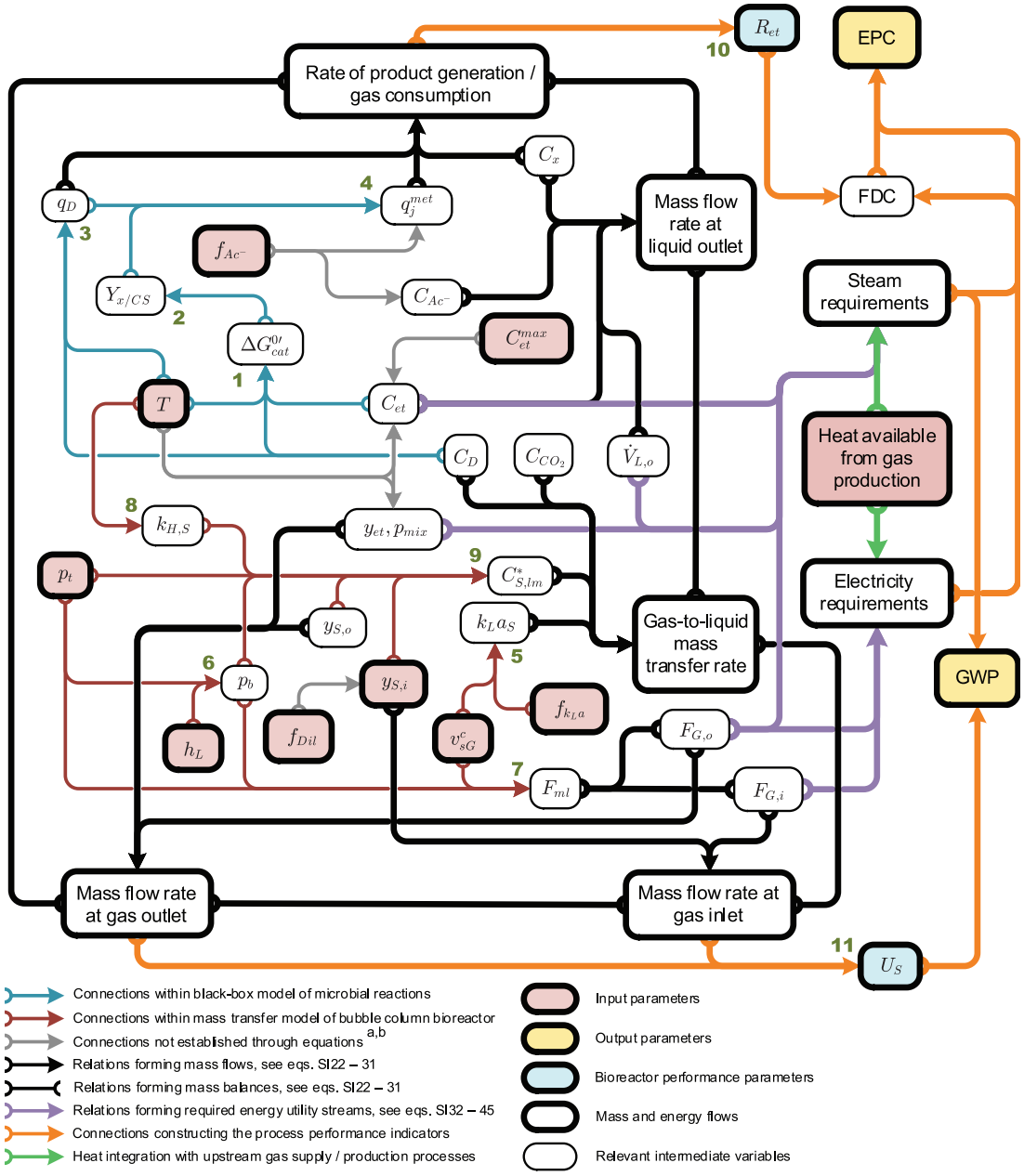

Fig. 2. Map of connections between the model's input and output variables. Numbers 1 to 11 represent the system of equation used as follow: 1: eq. SI1; 2: eq. SI2, SI3; 3: eq. SI4, SI5; 4: eq. SI6, SI7; 5: eq. SI8, SI9; 6: eq. SI14; 7: eq. SI11 – 15; 8: eq. SI16; 9: eq. SI17 – 19; 10: Eq. (20), (11), (21). See glossary above. [a]*IV*'s with indirect entrance to the model: f_{Ac^-} defines how much of the carbon directed towards ethanol and acetic acid, corresponds specifically to acetic acid, $f_{k_L a}$ multiplies the $k_L a$ estimated for pure water, f_{Dil} controls gas feed dilution with excess CO_2, C_{et}^{max} is introduced as an upper bound to constrain the ethanol concentration solutions within the bioreactor simulation (see Almeida Benalcázar et al., 2020a). The input parameter $y_{S,i}$ stands for the composition of the gas feed, it represents the different gas feedstocks used in the analysis, the BOF off-gas, the bio-based syngas and the H_2/CO_2 mixture. [b]NRTL-based vapor-liquid equilibria for the ethanol-water system (data gathered from Beneke, 2013).

the extra steam could be used for the production of electricity, the purchase costs of the turbine are too large. For the BOF and BBS cases, electric energy is supplied from the local grid, whereas the steam that is not heat-integrated is produced from LPG combustion (see units at the bottom-left in Fig. 1).

All the power required by the HAC process is wind-based (see units at the bottom-left in Fig. 1). In this process configuration, there is no power required for inlet gas compression since CO_2 and H_2 are both supplied at higher pressure than that at the bottom of the bioreactor (Harrison et al., 2009; Rey Porto et al., 2010; Rochelle, 2009). The energy required for the production of H_2 through water electrolysis is 141.3 MJ/kg_{H2} (Harrison et al., 2009).

2.3. Models and indicators for economic performance and environmental impacts

The overall process economic performance is evaluated using the ethanol production costs (EPC), while the environmental impacts are quantified through the GWP category. In addition, the CO_2 abatement costs (CAC) are used because it amalgamates the information of the GWP and the EPC and thus, (*i*) it provides a common ground for comparison between the different gas composition cases and (*ii*) it allows identifying the conditions where lowering either, the GWP or the EPC, is most relevant for decarbonizing ethanol production. Throughout the presentation and discussion of the results, the process performance of the gas fer-

mentation configurations are compared to fossil-based and second generation ethanol whose economic and environmental performance data is collected from CGEE (2017), Efe et al. (2005), Humbird et al. (2011), Millinger et al. (2018), Muñoz et al. (2014).

The economic and environmental performance indicators are calculated considering that the industrial facilities are located in Europe.

2.3.1. Calculation of the global warming potential

The calculation of the GWP follows a life cycle perspective with a cradle-to-grave approach, considering combustion as the end-of-life of ethanol. The GWP is the sum of the CO_2 equivalents emitted through: (*i*) the overall gas production stages, (*ii*) the generation of steam and electric energy (gathered from the local grid for BOD and BBS cases and derived from wind for the HAC case), (*iii*) the flaring of the bioreactor off-gas, (*iv*) the disposal of bacterial biomass and acetate through wastewater treatment (allocation by weight is used), and (*v*) the final combustion of ethanol. The components CO and CO_2 contained in the gas feedstocks of the BOF and the HAC cases are assumed to be avoided emissions that would otherwise be released to the atmosphere; therefore, for accounting purposes, the carbon in these streams is regarded as credits. The carbon contained in the syngas of the BBS case is instead biogenic. The credits as well as the biogenic carbon are subtracted from final GWP accounting.

Moreover, there are specific considerations for each gas feedstock regarding the emissions derived from their production stages:

- In the steel production process, the heat of combustion of the BOF off-gas is used at a first stage, the making of the sinter; according to the data presented by Burchart-Korol (2013), the flaring of the BOF off-gas contributes with the 0.11% of this stage's energy requirements, where most of the energy comes from coal and electricity (71 and 12%, respectively). Because of that fractional contribution of BOF off-gas, the emissions related to the production of the BOF off-gas, may be left as part of steel's GWP, as proposed by Handler et al. (2016); all the results presented in this study use this assumption. Another possibility for counting the GHG emissions related to the diversion of the BOF off-gas from the steel production without modifying the GWP of steel, is assigning the GWP of the extra electricity or coal needed for covering the energy gap left by the BOF off-gas (see a schematic representation of the process-level assignment of GHG emissions to the BOF off-gas Figs. SI1a and SI1b). The analysis of that possibility is included in the results (Section 3.1) assuming a GWP of 356 g_{CO2e}/KWh for coal (Ladage et al., 2021); the GWP of electric energy is shown below.
- In the HAC case, the emissions related to the production of H_2 and the capture of CO_2 are considered. The production of H_2 considers the contributions of the electrolysis of water and the compression of H_2 (213 g_{CO2e}/kg_{H2} Cetinkaya et al., 2012). The scrubbing of CO_2 includes the contributions of the chemicals used in the process plus the heat and wind-based power (25 g_{CO2e}/kg_{CO2} Grant et al., 2014).
- In the BBS case, the value 57.5 g_{CO2e}/kg_{syngas} (Almeida Benalcázar et al., 2017) considers biomass production and local transportation, drying and syngas production. The same value also considers that part of the steam needed by the gasification is produced by heat integration with syngas cooling.

Due to low contributions, the assessments neglects the nutrients and bases (for pH control) in the fermentation, water consumption (since a large reuse stream is used, see line 7 in Fig. 1), the construction of the electrolyzer and, the distribution of the fuel to the final consumers (Almeida Benalcázar et al., 2017; Handler et al., 2016; Mehmeti et al., 2018).

The production of steam and electric energy for the BOF and BBS cases generate 189 and 101 kg_{CO2e}/GJ (Almeida Benalcázar et al., 2017), respectively. On the HAC case, the electric energy produced by wind turbines generates 2.8 kg_{CO2e}/GJ (Caduff et al., 2012).

2.3.2. Calculation of the ethanol production costs

The EPC include the contributions of both, variable and fixed costs. The EPC are thus the sum of the expenses related to: (*i*) the production of the gas feedstock on the HAC and BBS cases, (*ii*) the generation of steam and electric energy, and, (*iii*) the facility dependent costs. The costs of the utilities and the gas feedstocks are presented in Table 3. The production costs of the BOF off-gas are determined using the costs of the equivalent amount of electric energy needed by the production of the sinter in the steel production process; this is the cost of the BOF-gas used for the estimation of all the results presented in this study. However, similar to the assignment of the GWP to the BOF off-gas, the production costs of the gas feedstock depend on what is assumed to be the replacement of the BOF off-gas at the steel production process. Therefore, a discussion is presented in the results (Section 3.1) about the consequences of assigning the costs of the equivalent amount (in energetic terms) of coal to the costs of BOF off-gas. The cost of coal is taken as the five-year average of 54 EUR/ton presented in euracoal.eu.

Due to low contributions, the cost accounting neglects the costs related to the nutrients, alkalis and water consumption in the fermentation (Almeida Benalcázar et al., 2017).

The facility dependent costs (FDC) are assumed to represent the 10% of the CAPEX, which is in turn calculated by multiplying the total purchase costs of main industrial equipment by 6.8. The two latter simplifications are assumed based on the results reported in Almeida Benalcázar et al. (2017). The purchase costs of the off-gas condensers, flash separation drums and the distillation columns are gathered from Aspen Plus v8.8; the cost of the bioreactor is taken from Almeida Benalcázar et al. (2017); the costs of the gas compressors (C1 and C2 in Fig. 1) are obtained from Seider et al. (2010). The purchase costs of the ethanol dehydration unit, the H_2 and syngas production facilities, as well as the heat recovery boiler that produces steam from the cooling of the gas feedstocks are adapted from reported techno-economic assessments (see Table 3). All the purchase costs are corrected for capacity and year by using a scaling factor of six-tenths (Peters and Timmerhaus, 1991) and adjusted by inflation to 2019 with the chemical engineering plant cost index (Access Intelligence LLC, 2019) (see Table SI7), respectively; and lastly, those costs that are found in USD in literature, are converted to a 2019 EUR by multiplying by a factor of 0.885.

2.3.3. CO_2 abatement costs

The CAC are considered as the costs of reducing GHG emissions through the production and use of gas fermentation-based ethanol compared to fossil-based gasoline (see Eq. (9)). The GWP of gasoline is assumed as 83.8 g_{CO2e}/MJ (which considers oil extraction and refinement into gasoline plus its combustion) (European Parliament, 2009). The units of CAC are €/ton_{CO2e}.

$$CAC = \left(\frac{EPC}{GWP_{gasoline} - GWP_{ethanol}} \right) \cdot 1000 \tag{9}$$

2.4. Sensitivity analysis

Due to the non-linear relation between the model's *IV*'s and *OV*'s, a non-parametric method is used for assessing the sensitivity of the EPC, the GWP and CAC to the model *IV*'s. The sensitivity is assessed by the Monte Carlo filtering method (Burhenne, 2013; Saltelli et al., 2007), which consists of, first, a stochastic (Monte

Table 3
Cost data about utilities, raw materials and purchase cost data for processing units based on techno-economic assessments reported in literature.

(a) Costs of utilities and raw materials

Utility/raw material	Cost [€]	Functional unit	Used in case	Refs.
Steam production	22.30	GJ	BOF, BBS	Almeida Benalcázar et al. (2017)
Purchase of electric energy from local grid	13.72	GJ	BOF, BBS	Efe et al. (2005)
Acquisition of biomass plus the production of syngas	120.35	ton of syngas	BBS	Almeida Benalcázar et al. (2017)
Wind-based electric energy [a]	4.92	GJ	HAC	IRENA (2019)
CO_2 scrubbing [b]	37	ton of CO_2	HAC	Husebye et al. (2012)

(b) Purchase costs of processing units

Processing unit	Cost [€]	Year	Reference capacity	Refs.
Ethanol dehydration plant	2.75×10^6	2000	24,564 $kg_{ethanol}/h$	Aden et al. (2002)
Heat recovery boiler	1.57×10^7	2001	891 kg_{gas}/s	Kwak et al. (2006)
Alkaline water hydrolysis based hydrogen production plant	4.40×10^6	2017	90 kg_{H2}/h	Yao et al. (2017)
Amine based CO_2 capture plant	1.25×10^8	2012	70.2 kg_{CO2}/s	Husebye et al. (2012)
Biomass gasification plant [c]	7.22×10^7	2017	51,892 kg_{syngas}/h	Almeida Benalcázar et al. (2017)

Note: Find the detailed purchase costs estimated for all process equipment and plants for the three gas supply options on Table SI6.
[a] For the HAC case, the specific cost related to the production of H_2 is reported as 'gas production costs' because, although the cost item is part of the electric energy costs, the differentiation allows comparing the cost of the gas feedstock with the BOF and BBS cases.
[b] It is assumed that the concentration of CO_2 in the flue gas is 20%v/v.
[c] Purchase costs include the tar reforming unit as part of gas cleaning.

Carlo) process simulation using 5000 randomly generated combinations of the eight model *IV*'s for each of the three gas composition cases (the final number of simulations is 15,000). The total number of simulations for each case is subsequently divided into two subsets according to a base criterion: belonging to the 10% best performing simulations according to each *OV*. This subset is called the behavioral subset, while the rest of the simulations form the non-behavioral subset. One behavioral subset is obtained for each *OV* by choosing the 500 simulations that independently produced the lowest GWP, or EPC, or CAC.

The sensitivity (S) of one *OV* to each *IV* is identified by the difference between the distribution of each *IV* in the behavioral subset ($\bar{B}$) and the distribution of the same *IV* in the non-behavioral subset (B). The *OV*'s sensitivity to the specific *IV* is proportional to the difference in those distributions (Burhenne, 2013; Saltelli et al., 2007). The difference in the distributions is visualized in plots of the empirical cumulative distribution functions (ECDF's) and quantified using the Smirnov's statistical two-sample test (Saltelli et al., 2007) (see Eq. (10)), which is based on the estimation of the maximum difference ($d^{B-\bar{B}}$) between the ECDF's of the B and $\bar{B}$ subsets. For comparison between the sensitivities of different *IV*'s, $d^{B-\bar{B}}$ is normalized by dividing it by the difference between the high and the low limits within which, each specific *IV* was varied (see Table 4).

$$d^{B-\bar{B}}_{IV_i,OV_j} = \max\left(\left|\mathrm{ECDF}(B) - \mathrm{ECDF}\left(\bar{B}\right)\right|\right) \tag{10}$$

The upper and lower limits used for the eight *IV*'s are shown in Table 4. The limits are based on information reported in literature; such information is also shown in Table 4.

2.5. Process optimizations

The process optimizations simultaneously minimize two objective functions, the GWP and the EPC; the decision variables are the model's *IV*'s. The GWP and the EPC are often conflicting indicators, therefore, the optimization ends in the construction of Pareto frontiers. To identify potential environmental and economic gains of future developments on strain modifications for higher selectivity and tolerance to ethanol, as well as a more delicate control of the gas feedstock dilution, the multi-objective optimizations are organized into two steps. The first step consists of finding an 'ideal' set of *IV*'s for each process configuration; in this step, the optimization is constrained by the *IV*'s lower and upper limits, as shown in Table 4. The second step on the other hand, considers that f_{Dil} will not be lower than 15% (a common dilution of syngas and BOF off-gas Bieda, 2012; Ciferno and Marano, 2002), f_{Ac-} is fixed at 0.05 (a selectivity claimed by LanzaTech on their reactors Simpson, 2018), C_{et}^{max} will not be higher than 50 g/L (the maximum ever reported for a gas fermentation Phillips et al., 1993) and mass transfer coefficients will not surpass those estimated for transfer into pure water by more than 50% ($f_{k_La} < 1.5$, possibly attained with a 50 g/L ethanol solution Sun et al., 1988). The second step finds more 'realistic' solutions. Lastly, since it has been recently suggested that ethanol inhibits the consumption of the electron donors (de Medeiros et al., 2019), an inhibition term is added to the kinetic equation for electron donor uptake (see Eq. (11)) to perform the optimizations under the 'realistic' conditions. The inhibition constant ($K_{I,et}$) equals 500 mM (value estimated with a thermodynamic-metabolic model currently under construction).

$$q_D = q_D^{max}\left(\frac{C_D}{K_D + C_D}\right)\left(\frac{1}{1 + \frac{C_{et}}{K_{I,et}}}\right) \tag{11}$$

The calculation is performed by an elitist genetic algorithm implemented into the function 'gamultiobj' in MatLab R2017b. According the software documentation, the function is a variant of the 'non dominated sorting genetic algorithm II' (NSGA-II) (Deb, 2001) which has previously been used for optimizing operation parameters of mechanical machines (Yusoff et al., 2011).

3. Results and discussion

This section starts with a description of the general distributions of the GWP, the EPC and the CAC obtained from the stochastic simulations of the three proposed process configurations. The latter assessment is followed by the sensitivity analysis using the Monte Carlo filtering method and ends with an elaboration on the results from the multi-objective optimizations.

3.1. Distribution trends in the performance indicators

Fig. 3 shows boxplots with the distributions of the GWP, the EPC and the CAC for the three process configurations. The boxplots show the median values of the indicators, as well as the 5th, 25th,

Table 4
Variation limits of the IV's.

IP	Low limit	High limit	Comments about the selection of the limits
T [°C]	25	67	Range based on the diversity of optimal growth temperatures reported for acetogens (Drake et al., 2008).
p_t [atm]	0.5	3.5	No comment
f_{Dil} [%vol.] [a]	0	45	The upper limit is based on the data reported for the BOF off-gas and syngas compositions (Bieda, 2012; Ciferno and Marano, 2002).
C_{et}^{max} [g/L]	30	120	The upper limit is based on reported data for ethanol production with *Saccharomyces cerevisiae* (Kechkar et al., 2019) (disregarding limitations of currently known bacterial strains).
h_L [m]	8	64	The upper limit is selected considering reported dimensions of air-lift bioreactors (Verlaan, 1987) (disregarding possible limitations in legislation, construction costs and safety).
f_{k_La} [-]	0.5	2.0	The limits are selected considering that surfactants could reduce the k_La estimated for gas transfer to pure water by 50% (Vasconcelos et al., 2003), and in contrast, the presence of ethanol (Guo et al., 2017) added to possible effects of granulated biofilms formation (van den Heuvel et al., 1995) might double the value of k_La from the value estimated for gas transfer to pure water.
f_{Ac^-} [-]	0.00	0.15	The limits are selected considering that the highest reported selectivities for ethanol lay between 85 and 95% (Kundiyana et al., 2010; Richter et al., 2013).
v_{sG}^c [m/s]	0.04	0.30	The lower and upper limits are chosen considering the on-set of the heterogeneous bubbling regime (Heijnen and Van't Riet, 1984) and the maximum value for the gas hold-up in bubble columns (Van't Riet and Tramper, 1991), respectively.

[a] The dilution of the feed was not applied to the HAC case because it is assumed that the gas feed composition could be finely adjusted from the pure H_2 and CO_2 streams.

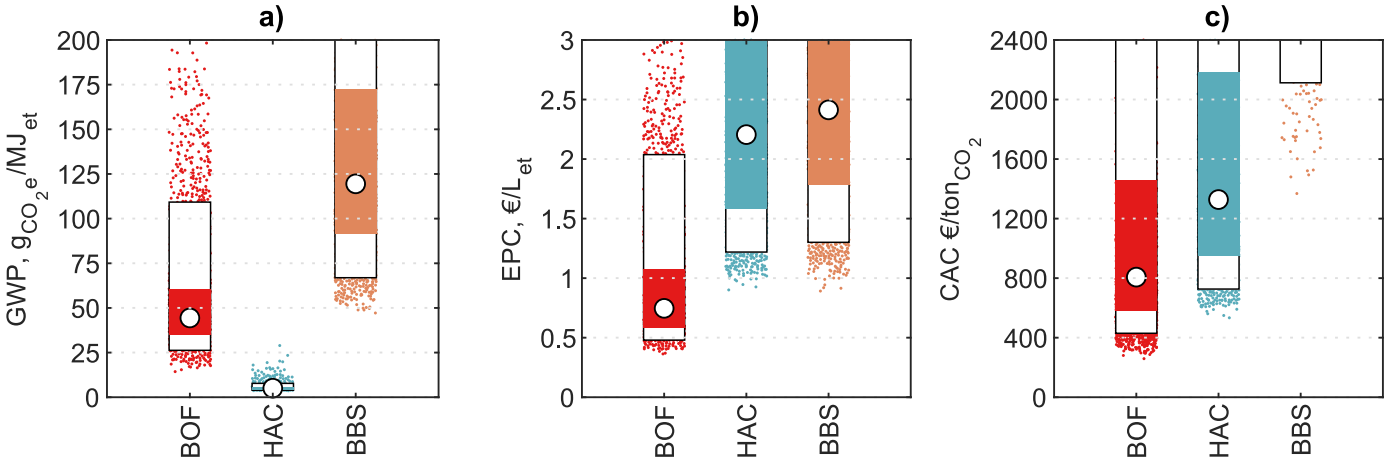

Fig. 3. Distribution of the (a) global warming potential, (b) ethanol production costs and (c) the relative CO_2 abatement costs from the stochastic simulations. On the boxplots: the colored vertical rectangles represent the extension of the 25th and 75th percentiles; the white vertical rectangles represent the extension of the 5th and 95th percentiles; the small colored dots represent the outliers; and the white circles represent the median values. The CAC plot was created neglecting the negative values obtained for the cases where the GWP was higher than that for fossil-based gasoline.

75th and the 95th percentiles of their distributions. The trends obtained for the three process configurations are used to compare their performances between each configuration and with data reported in literature for second generation ethanol and for fossil-based ethanol and gasoline.

The results suggest that the ethanol produced from BOF off-gas and the H_2/CO_2 mixture has high probabilities of improving the GHG emissions related to the fossil-based ethanol (Muñoz et al., 2014) and gasoline (European Parliament, 2009) (GWP of 138 and 83.3 g_{CO2e}/MJ, respectively). Ethanol produced from syngas has lower probabilities compared to the BOF and the HAC cases. However, only the BOF off-gas fermentation has a 25% probability of achieving production costs that are competitive with second generation ethanol (0.51 €/L CGEE, 2017). In the BOF case, the EPC may even be lower (reaching a median of 0.45 €/L) if the production costs of the BOF off-gas were taken as the costs of the equivalent amount of coal needed by steel production to fill the gap left by diverting the BOF off-gas to the fermentation.

The large amounts of sensible heat available for integration in the BOF off-gas, added to the absence of gas production facilities, led this process configuration to achieve the lowest EPC of three process configurations (see Fig. 4b). Additionally, the base-case consideration that the carbon content in the BOF off-gas represents credits for the production of ethanol leaves the GWP of the process dependent only on the emissions generated by the consumption of the electric energy and the steam that is not be covered by heat integration. These two indicators altogether lead to the lowest CO_2 abatement costs of the three cases, becoming the only case with significant probabilities of competing with the CAC of second and first generation ethanol, 584 and 332 €/ton_{CO2} (Millinger et al., 2018), respectively.

If alternatively, the GWP assigned to the BOF off-gas was taken as that of the extra energy inputs required to fill the energy gap left by the off-gas in the steel production process, the final GWP of ethanol would be much higher than that estimated with the use of credits, *i.e.*, the ethanol GWP will reach median values of 498 and 914 g_{CO2e}/MJ_{et} if the extra energy at steel production came from coal or electricity, respectively. This result suggests that the environmental impacts linked to ethanol produced from the BOF off-gas heavily depends on the modifications made at the steel production process. A potential feasible solution may be achieved by using a renewable and low-carbon source of electricity for steel production, for instance wind, which would bring the GWP of ethanol to a median of 53 g_{CO2e}/MJ_{et}.

The GWP and the EPC of the HAC case receive a similar benefit from the use of waste CO_2 compared to the BOF case *i.e.*, the GHG emissions are reduced by the use of credits; a similar result would be produced if the CO_2 was biogenic. However, the HAC case pro-

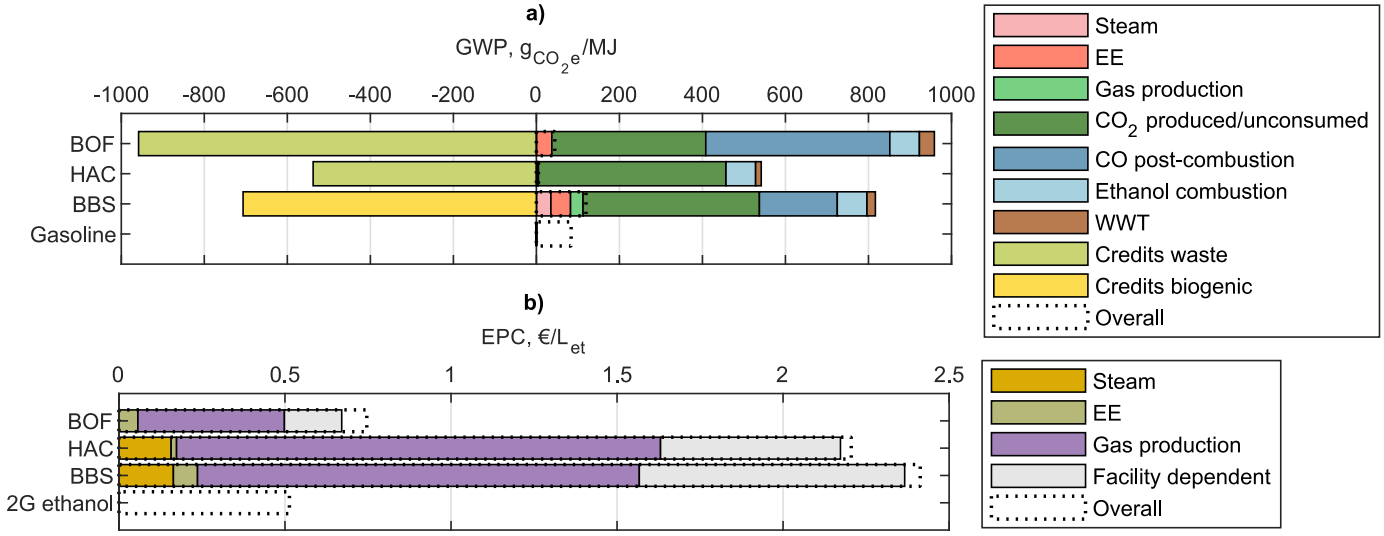

Fig. 4. Median values of the itemized contributions for (a) GWP and (b) EPC for the three process configurations. Gasoline is given a GWP equal to 83.3 g_{CO2e}/MJ, while 2G ethanol production costs are taken as 0.51 €/L (CGEE, 2017).

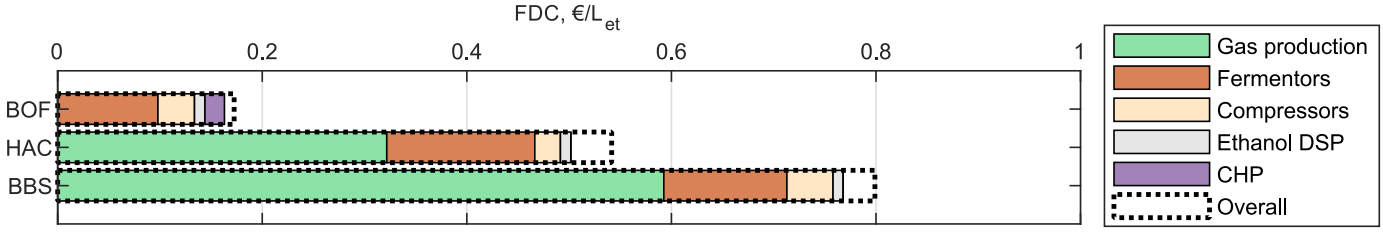

Fig. 5. Median values of the itemized contributions to the facility dependent costs (FDC) of the three process configurations.

duced higher EPC's than the BOF case due to the costly production of H_2 and the capture of CO_2.

The fermentation of the bio-based syngas produced the least promising results of the three considered process configurations. This result is derived mainly from the large costs of the gasification facilities (see Fig. 5), which are also relatively expensive to operate (see Fig. 4) for producing a gas feedstock whose energy integration capabilities are limited by the temperature (lower than the BOF off-gas) and the steam requirements of the gasification process itself. If instead, bio-syngas was purchased as a utility, within a large industrial complex that benefits from the economy-of-scale, the EPC may be considerably lower than in Fig. 4; an analysis of this possibility is shown in Section 3.3.3.

Altogether, the BOF and the BBS cases have a similar cost distribution between fixed and variable costs as 2G ethanol production, where 30% corresponds to fixed costs and 70% to variable costs (Humbird et al., 2011). The gas production costs have a particularly large contribution on the HAC case, where it sums up 66% of the total EPC, while the fixed costs represent 25% of the EPC. The economic burden of the facility dependent costs would also be lower if the ethanol production throughput was larger (taking advantage of the economy-of-scale) than the 220 kton/y assumed in this study.

Moreover, it has been previously argued that ethanol produced from BOF off-gas and BBS fermentations would have GWP's of 31 and 12 $g_{CO2e}/MJ_{ethanol}$, respectively (Handler et al., 2016). Since no details are given in that study about the bioreactor configuration, ethanol yields, production of cells, acetate co-production or on GHG emissions during the gasification of lignocellulosic biomass, it is therefore not possible to draw comparisons with the present study from that technical perspective. However, the GHG emissions accounting in that study gives credits to the energy savings due to the heat integration with the combustion of biogas produced by the wastewater treatment process. If those specific GHG emissions credits were applied in the present study, the GWP of the BOF off-gas and the H_2/CO_2 cases would have had negative values within their distributions. That result could have been misleading since negative GHG emissions, or CO_2 sequestration, have only been acknowledged for the creation of grasslands, forests and geological formations, as well as for the use of enhanced agriculture management and the injection of CO_2 into the oceans in the form of carbonates (Majumdar and Deutch, 2018). Therefore, it may be presumed that if the GHG emission credits due to heat integration were not counted in Handler et al. (2016), their results would have been comparable with the ones obtained in this study. That comparison may be used for further validating the accuracy of the estimations made by the gas fermentation model presented in Almeida Benalcázar et al. (2020a).

Furthermore, since the end use of the produced ethanol is combustion, the GHG emissions from the process where the BOF off-gas is generated (steel manufacture) are not mitigated by ethanol production. The energy contained in the gas may instead receive a better use when producing ethanol than when producing electric energy after being combusted. If the ultimate use of the gas was powering electric vehicles, then the gas-to-wheel efficiencies may be used as comparison basis to determine if the production of ethanol as fuel is worth the effort. For comparison, the analysis includes the HAC and BBS cases as well. The gas-to-fuel efficiency (η_{G-F} in Eq. (12)) due to ethanol production can be as high as 56, 84 and 69% for the BOF, the HAC and the BBS cases, respectively; the latter efficiencies may represent an improvement from corn ethanol and may be competitive with cellulosic ethanol, butanol and Fischer-Tropsch-based diesel (Huang and Zhang, 2011). After ethanol is used in a hybrid electric vehicle (fuel-to-wheel

efficiency of 31% Huang and Zhang, 2011), the gas-to-wheel efficiencies become at most 17, 26 and 22% for the BOF, the HAC and the BBS cases, respectively. On the other hand, if the BOF off-gas and the syngas were instead used to produce electricity and then that electricity was used to power the vehicles, the gas-to-wheel efficiencies will be 24% (electricity production from gas combustion efficiency is 35% (Handler et al., 2016) while the energy efficiency of electric cars is 68% (Huang and Zhang, 2011)), which is higher than that obtained by using the ethanol from the BOF off-gas and from syngas. A similar result is obtained if the H_2 was instead used directly by fuel-cell vehicles where the gas-to-wheel efficiency may reach 30%. Thus the use of ethanol produced from the HAC case may lead to higher gas-to-wheel efficiencies than using electric cars powered by energy derived from the combustion of BOF off-gas and syngas, but it may not improve that efficiency of directly using H_2 in fuel-cell vehicles. However, the perceived risks on the transportation and storage of H_2 (Kurtz et al., 2019), traditional safety concerns about using H_2 in passenger vehicles (The International Consortium for Fire Safety, Health and The Environment, 2011), despite the development of new and safe technologies (Euro NCAP, 2018), could undermine its widespread use in the near future and give opportunities to ethanol instead.

$$\eta_{G-F} = \frac{NCV_{et} \cdot Q_{et}}{NCV_{gas\ feed} \cdot Q_{gas\ feed}} \cdot 100\% \tag{12}$$

3.2. Sensitivity analysis by the Monte Carlo filtering method

The Monte Carlo filtering method is applied to qualitatively assess the sensitivity of the global warming potential GWP, the EPC and the CAC to the model *IV*'s. From the normalized maximum differences between the empirical cumulative distribution functions (ECDF) of the each *IV* in the behavioral and the non-behavioral Monte Carlo subsets, the level of sensitivity of the model *OV*'s is classified into three categories: high, medium and low sensitivities, assumed when the normalized $d^{B-\bar{B}} > 0.30$, when $0.29 > d^{B-\bar{B}} > 0.16$ and when $d^{B-\bar{B}} < 0.15$, respectively. Table 5 shows the results of this classification, while Fig. SI2 shows the ECDF plots.

The following sections trace the causes of the resulting sensitivities of the model *OV*'s to each *IV*, for the three gas supply options. Special attention is given to the effects of the estimated sensitivities on actual process development challenges.

3.2.1. Sensitivity of the global warming potential

The potential for energy integration of the different gas feedstocks determines the sensitivity of the GWP to the different *IV*'s. Since the temperature and pressure of the gas feedstocks are different for the three process configurations, the GWP shows different sensitivity trends for the three gas-feed options. What can be generalized for the HAC and BBS cases is that the GWP directly depends on the *IV*'s that influence the energy requirements of the gas compression and the distillation of ethanol, the two major requirements in the overall process. The shocks of the increases in energy requirements for the fermentation of the BOF off-gas are, differently than for the other gas feedstocks, buffered by the large amounts of energy available for integration in the gas feedstock. This feature of the BOF off-gas may be exceptionally beneficial since it causes a low sensitivity of the GWP to low ethanol concentrations and to low mass transfer coefficients, which in practice represent two relevant technological challenges of gas fermentations (Liew et al., 2016; Munasinghe and Khanal, 2010).

The power requirements for ethanol distillation are increased either when ethanol accumulations are low in the bioreactor or when most of the ethanol is withdrawn along the liquid outflow. The co-production of acetic acid demands a large outflow rate from the bioreactor to avoid its accumulation; similarly, temperature exponentially rises the rates of microbial substrate consumption (see Eq. (SI4)), which produces faster growth, and consequently demands higher liquid outflow rates from the bioreactor. Therefore, the GWP shows medium to high sensitivities to the T and the f_{Ac^-} for the three process configurations. The effect of increasing acetic acid co-production is particularly detrimental for the HAC case where biomass production rate is low, as well as the liquid outflow needed to withdraw the cells from the bioreactor; when f_{Ac^-} increases, the liquid outflow and the energy demands from the distillation increase largely (see Figs. SI7–SI9) due to a low concentration of ethanol in the bioreactor.

Increased temperatures may nevertheless be feasible if the biomass withdrawal from the bioreactor was decoupled from the fermentation broth outflow using unit operations such as filtration and centrifugation or other solutions like retaining cells within granular biofilms (Lettinga et al., 1980; Shen et al., 2017). However, such solutions may only be feasible for fermentations of CO-rich gases because as the T increases, the threshold concentrations of CO, H_2 and CO_2 increase as well (see Fig. SI11). Considering that the threshold for H_2 is two orders of magnitude higher than that for CO, the thermodynamic feasibility of the catabolism of H_2 may represent a limitation for achieving high U_S with H_2-rich gases, since the partial pressures of the electron donors will be low at the top of the bioreactor.

Moreover, the power employed for gas compression will fall with lower gas flow rates to the bioreactor; that is the case when the mass transfer coefficients are high. Contrarily, increased top reactor pressures, liquid column heights and superficial gas velocities would, in general, involve higher energy demands for gas compression. However, the characteristics of the gas feedstocks cause the appearance of exceptions to the higher energy demands for gas compression, an effect that for instance, would be completely avoided if the gas feedstock was produced at high pressures, as in the HAC case; for that reason, the GWP of the HAC will fully bene-

Table 5
Classification of sensitivity of the process performance indicators to each *IV* for the three process configurations.

OV	Gas supply option	*IV*							
		T	p_t	f_{Dil}	C_{et}^{max}	h_L	f_{k_La}	f_{Ac^-}	v_{sG}^c
GWP	BOF	0.41	0.25	0.42	-0.07	0.07	-0.41	0.26	0.24
	HAC	0.18	-0.23	n/a	-0.36	0.13	-0.17	0.77	0.09
	BBS	0.16	0.10	0.38	-0.17	-0.22	-0.32	0.52	0.33
EPC	BOF	0.10	0.12	0.34	-0.06	-0.50	-0.55	0.38	0.12
	HAC	-0.23	-0.21	n/a	-0.13	-0.37	-0.40	0.42	0.29
	BBS	-0.24	0.08	0.53	-0.07	-0.38	-0.36	0.34	0.29
CAC	BOF	0.07	0.05	0.05	-0.04	-0.04	-0.05	0.07	0.06
	HAC	-0.23	-0.21	n/a	-0.13	-0.36	-0.40	0.42	0.29
	BBS	0.10	0.07	0.40	-0.16	-0.28	-0.33	0.49	0.30

Note: The intensity of the green color in the cells represents the level of the absolute sensitivity; the darker tones represent higher sensitivities while the lighter tones represent lower sensitivities. The signs + and - indicate whether the *IV* increases or decreases the value of the *OV*, respectively.

fit from the improvements on the ethanol productivity induced by the increased liquid column heights and top bioreactor pressures.

In the BOF case, the increases in the liquid column height would raise the GWP because the improved productivity ends in a reduced demand for gas inflow to the bioreactor, cutting the heat integration potential of this gas feedstock.

Moreover, the dilution of the gas feed will cause a drop on ethanol productivity in the bioreactor (see Fig. SI6) and therefore, although the absolute energy requirements remain unaffected when productivity falls, the requirements relative to ethanol produced increase with dilution (see Fig. SI9), and so does the GWP for the BOF and BBS cases. The GWP in the HAC case is not affected because dilution is not considered an option because the gas feed composition can be finely adjusted.

3.2.2. Sensitivity of the ethanol production costs

The EPC in the three process configurations have a highly negative sensitivity to the *IV*'s that influence the ethanol productivity in the bioreactor, variables that directly determine the number of bioreactors needed to achieve the desired ethanol throughput (see Fig. SI5b). Thus, the EPC in the three process configurations is greatly reduced by increases in f_{k_La} and h_L; contrarily the EPC will expand by increases in the f_{Dil} and in the f_{Ac^-}.

One exceptional case is the effect of v^c_{sG} on the EPC. While increases in the v^c_{sG} will raise R_{et} (see Fig. SI6a) and will therefore reduce the fixed costs related to the bioreactors (see Fig. SI5b), it will also cause an increase on the size of the gas compressors (see Fig. SI5c), ultimately rising the overall FDC. These effects of increasing v^c_{sG} are further aggravated by the higher costs related to the production of the gas feedstock and the higher energy demand for gas compression (see Figs. SI4c and SI4d).

3.2.3. Sensitivity of the CO_2 abatements costs

Since the CO_2 abatement costs are calculated using the GWP and the EPC, the sensitivities of the latter parameters are partially transferred to the CAC. However, the large sensitivities on the cases where the EPC and the GWP have narrow distributions from the Mote Carlo simulation, are not transferred to the CAC. This is precisely the case for the CAC sensitivity on the H_2/CO_2 fermentation, which receives the sensitivity only from the EPC and not from the GWP, which for this process configuration is exceptionally low.

For the case of the BOF off-gas fermentation, the CAC is not sensitive to any of the *IV*'s; the reason for this result is the generally low GWP values (as in the HAC case), and a cancelling effect produced by the combination between a highly negative with highly positive sensitivity observed for the increases in the liquid column height.

On the BBS case, the CAC is largely sensitive to T because it severely rises the already high value of the GWP, which for a large fraction of the Monte Carlo scenarios is higher than gasoline's GWP, thus making the CAC negative. The CAC's sensitivities for the rest of the *IV*'s are the result of compensatory or additive effects between the sensitivity levels of GWP and EPC. In general, the CAC shows sensitivity to the *IV*'s that affect the energy requirements for distillation and gas compression (p_t and h_L), the bioreactor productivity (f_{Dil}, h_L, f_{k_La} and f_{Ac^-}) and the demand of the gas feedstock (f_{Dil} and v^c_{sG}).

3.3. Multi-objective process optimizations

This section describes each optimized process configuration under the 'ideal' and the 'realistic' conditions; the description is made for each process configuration independently. Figs. 6 and 7 show the specific values of the *IV*'s and *OV*'s obtained for each optimized case, respectively.

3.3.1. The optimized BOF case

In general, the simultaneous optimization of the EPC and the GWP applied to the fermentation of BOF off-gas produced a system that minimizes the gas production costs and the facility dependent costs. The gas production costs are minimized by the maximization of gas utilization (U_S), while guaranteeing that the overall process steam requirements are covered by the heat integration with the minimized gas feedstock inflow to the bioreactor. The EPC is maximized only on the cases where the bioreactor productivity (R_{et}) is maximized. The higher R_{et} is translated to lower FDC, but it also generates a higher demand of electric energy for the compression of higher gas flow rates, thus raising the GWP. This trend of the configuration of the Pareto frontier is seen in the optimizations under the 'ideal' and the 'realistic' conditions (see Fig. 7a and d).

As shown in Fig. 6a and d, the optimization under 'ideal' conditions favors the energy integration to compensate the higher steam demands caused by the higher ethanol productivities at the bioreactor. A gas feed dilution between 14 and 23% balances the energy that can be recovered from the gas feedstock with the R_{et} improved by a mass transfer coefficient factor at 2 and a temperature between 40 and 45 °C.

The Pareto frontier is formed by a balance between R_{et} and the steam requirements from the distillation of ethanol. In the bioreactor, there is a direct relation between R_{et} and the amount of ethanol that exits the bioreactor along the liquid outflow and consequently, the relationship extends to the steam requirements from the distillation. The top bioreactor pressure, the gas feed dilution and the height of the liquid column define the Pareto frontier *i.e.*, the p_t, the f_{Dil} and the h_L are at 0.9 atm, 14% and 33 m, respectively when the GWP is minimum, whereas p_t, the f_{Dil} and the h_L fall in 2.5 atm, 23% and 63 m, respectively when the EPC is minimum. For both configurations, the ethanol concentration in the bioreactor does not overpass 32 g/L; on the GWP Pareto optimum, due to the low pressure and on the EPC Pareto optimum, due to the high gas outflow rate from the bioreactor caused by the larger dilution of the gas feed. Overall, the two points (GWP, EPC) forming the 'ideal' Pareto frontier are (13.8, 0.50) and (21.9, 0.37) in units g_{CO2e}/MJ_{et} and €/L_{et}, respectively (see Fig. 7).

In the optimization under the 'realistic' conditions, R_{et} is highly affected by ethanol inhibition, however, this process configuration takes the advantage of the low contribution of the facility dependent costs to the overall EPC of the BOF case. One consequence of the reduced R_{et} is the reduced demand for gas feedstock, which contributes to keeping low costs related to the gas supply; other minor consequences are the reduced energy demand for gas compression and for the distillation of ethanol. Overall, the EPC climbs to 0.48 €/L_{et} in its Pareto optimum (see Fig. 7a).

The above mentioned 'realistic' EPC makes the BOF off-gas, the most economically attractive gas feedstock of the three considered in this study. However, the generation of the BOF off-gas in the world is limited by the steel throughput; approximately 217 × 10^9 L of ethanol could be produced per year if the BOF off-gas from all the steel production plants in the world was used (assuming that (*i*) all these plants use the basic oxygen furnaces, (*ii*)65 m^3 of BOF off-gas is generated per ton of steel (Bieda, 2012), (*iii*) 0.5 m^3 of BOF off-gas is required per L of ethanol and considering that 1808 Mton of steel are produced in one year World Steel Association, 2019). Such yearly production is equivalent to the 228% of the 2014 global production of ethanol (CGEE, 2017) and is also equivalent to a 13.7% of the global consumption of gasoline and jet fuel during 2018 (Plc, 2019) (the fuel consumption data was corrected with the ratio between the lower heating values of ethanol and gasoline). Therefore, although the use of BOF off-gas to produce ethanol through its fermentation would have CO_2 abatement costs as low as 269 €/ton_{CO2} (see Fig. 7c), it would

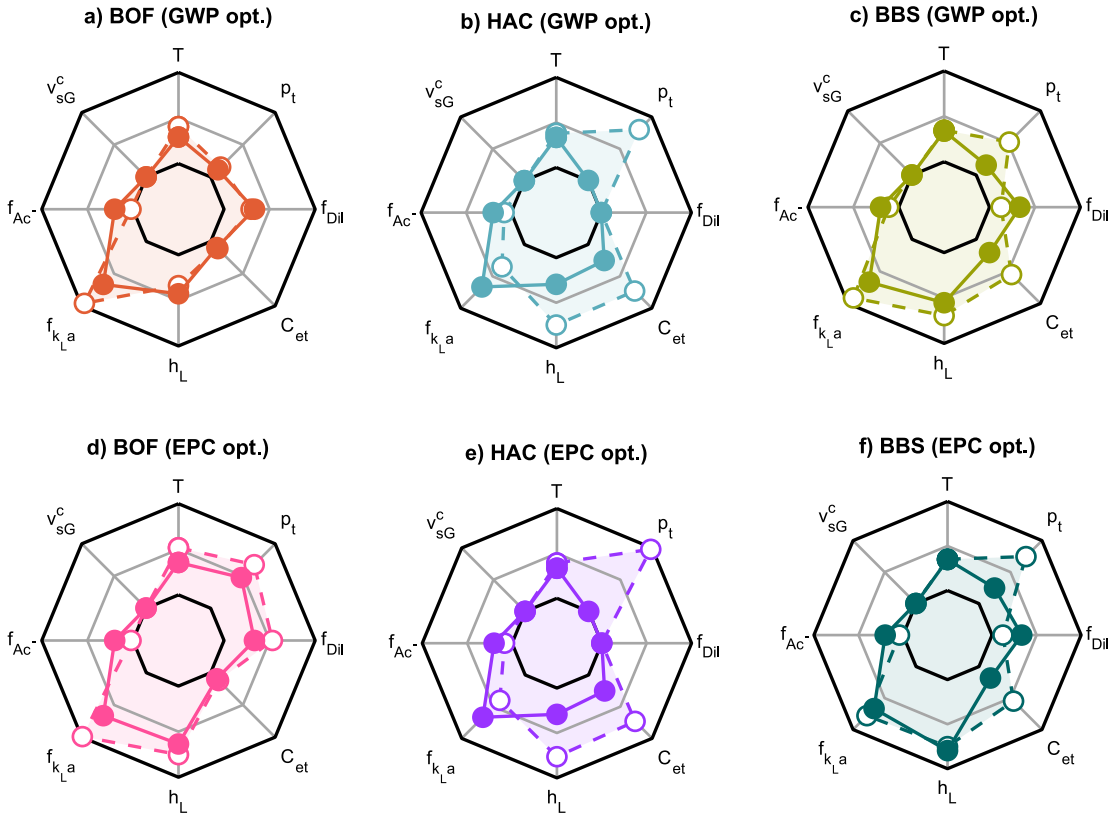

Fig. 6. Combinations of *IV*'s describing each optimized process configuration: (a), (b) and (c) correspond to the BOF off-gas, H_2/CO_2 and the BBS cases, respectively, where the GWP is at the Pareto optimal; (d), (e) and (f) correspond to the BOF off-gas, H_2/CO_2 and the BBS cases, respectively, where the EPC is at the Pareto optimal. The white and the fully colored circles represent the data for the optimized cases under the 'ideal' and the 'real' conditions, respectively.

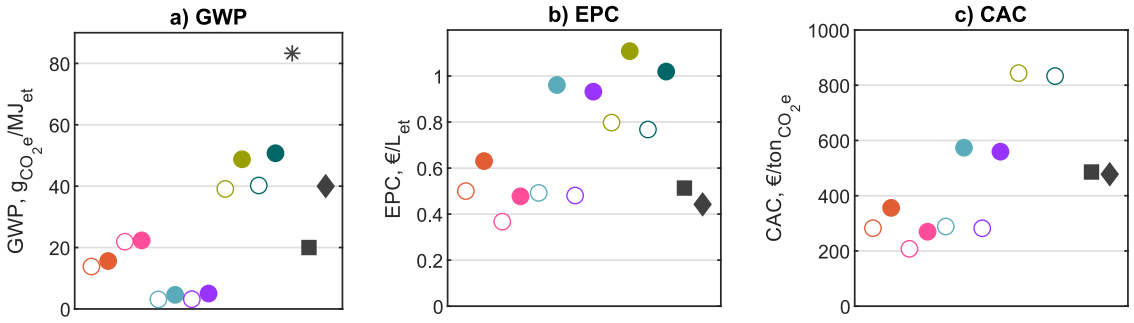

Fig. 7. Pareto optimal *OV*'s for each process configuration: (a) global warming potential, (b) ethanol production costs and (c) the CO_2 abatement costs. The white and the fully colored circles represent the data for the optimized cases under the 'ideal' and the 'real' conditions, respectively. The asterisk represents the GWP of fossil-based gasoline whereas the black squares and the black diamonds represent the performance of 2G and 1G ethanol, respectively. In the plots showing the *IV*'s values, the black colored outer and inner radial axes represent the highest and the lowest values of the *IV*'s as shown in Table 4. The specific data used to construct the plots is shown in Table SI5 at the SI.

not completely displace the equivalent fossil-based fuels in the transportation sector due to a limitation on the availability of the feedstock.

3.3.2. The optimized HAC case

The optimization of EPC in the HAC case was solved for a bioreactor configuration that reduces the excessively high costs related to the production of the gas mixture and to the investment on the H_2 and CO_2 production facilities. Such performance is achieved by simultaneously maximizing R_{et} and U_S up to a point where the concentration of H_2 at the top of the bioreactor does not achieve its thermodynamic threshold. Here, the gas recycling scheme comes in handy because achieving $U_S > 50\%$ are not necessary, while it is for the other gas supply options to avoid wasting the valuable gas feedstock. At the same time, the already low GWP is minimized by reducing the energy demands of the distillation and those of the gas outflow compression (for gas recycle). The combinations between the *IV*'s to achieve those performance trends depend on whether the optimization is made under the 'ideal' or the 'realistic' conditions. There are however, two common *IV*'s for all the optimum points *i.e.*, a process temperature between 37 and 40 °C and a low superficial gas velocity between 4.2 and 6.8 m/s. Such T balances the potential gains in productivity with the consequential increases on steam requirements by the distillation, while v^c_{sG} causes an improved gas utilization at low energy requirements for its compression.

The optimization under the 'ideal' conditions achieved an EPC between 0.48 and 0.49 €/L_{et} (see Fig. 7); that is about 49% lower than the EPC estimated for the 'realistic' conditions. The potential economic gains of further research are thus large in this process configuration. The 'ideal' process conditions that may sustain the low EPC are two: the ethanol concentration of around 93 g/L and a top pressure between 2.9 and 3.4 atm. The high p_t allows the maximization of R_{et} while avoiding reaching H_2 threshold at the top of the bioreactor and takes advantage of the already pressurized gas feedstocks to avoid increases on costs and emissions due to gas compression. The high ethanol concentration, possible thanks to the low acetic acid co-production and the low biomass yield caused by H_2 catabolism, reduces the emissions at the distillation. Last, the optimized mass transfer coefficient factor is close to 1, implying that the ethanol productivity is maximized only by p_t and h_L, while the low f_{k_La} (along with the high p_t) assures that the H_2 threshold is not achieved at the top of the liquid column.

The optimization under 'realistic' conditions suffers from a very low ethanol productivity in the bioreactor (see Table SI5), caused by the inhibitory effect of ethanol, whose concentration is estimated at 45 g/L. The main consequence of the low R_{et} is the doubling of the facility-dependent costs, compared to the 'ideal' optimization. To minimize costs and the GWP, the 30 m high bioreactor operates at a p_t of 0.5 atm to reduce U_S and allow higher gas outflow rates to remove larger amounts of ethanol from the liquid phase. This configuration reduces the burden on the distillation while increasing the energy demand for the compression of the gas recycle. The EPC thus falls between 0.93 and 0.96 €/L_{et} under the described configuration (see Fig. 7).

To make the ethanol produced from the fermentation of H_2/CO_2 at the 'realistic' conditions able to compete with second generation ethanol (0.51 €/L CGEE, 2017), large improvements on ethanol productivity may have to be achieved. The optimization suggests that the main objective of these improvements should be mitigating ethanol inhibition.

3.3.3. The optimized BBS case

Under the 'ideal' conditions, the bioreactor maximizes U_S by a tall liquid column of 60 m and a low superficial gas velocity of 6 cm/s (see Fig. 6c and f); R_{et} is on the other hand, maximized by a low dilution of the gas feedstock and a high mass transfer coefficient (see Fig. 6c and f). The Pareto frontier is formed, similar to the BOF case, by a balance between R_{et} and the energy requirements of the distillation. A p_t of 2.7 atm minimizes the EPC to 0.77 €/L_{et}, however, raising the costs related of the distillation. A p_t of 2.0 atm reduces the load of the distillation columns, minimizing the GWP to 39 g_{CO2e}/MJ_{et} but compromising the facility-dependent costs due to the reduction on R_{et}.

The severe reduction on productivity caused by the ethanol inhibition and the gas feed dilution in the optimization at 'realistic' conditions, increases the FDC by 50% compared to the optimization under 'ideal' conditions. Overall, a liquid column between 49 and 66 m, plus a superficial gas velocity of 8.5 cm/s aim to reduce the gas inflow rate, thus maintaining low gas production costs and low facility-dependent costs related to gas production. At the same time, the R_{et} reduced by ethanol inhibition and the low p_t (1.0–1.2 atm) increases the purchase costs of fermentors, but it also maintains low steam requirements at the distillation.

The EPC and the GWP estimated by the optimization of the BBS process under the 'realistic' conditions are 1.02 €/L_{et} and 48.8 g_{CO2e}/MJ (see Fig. 7). With such performance, the ethanol may not be competitive with second generation ethanol unless further optimizations are made on the biomass supply chain and the gas production process, by far the major contributors to EPC. For instance, ethanol from BBS fermentation may compete with 2G ethanol if *(i)* the syngas production costs were lowered by 60% to 0.51 €/kg_{BBS} and *(ii)* the investment for the gasification plant were also lowered 60% from what is reported in Table 3.

Lastly, using the results from the optimization at the 'realistic' conditions, the improvements derived from using wind energy and if the bio-syngas was purchased as a utility inside a large industrial complex (FDC cost of the gasification plant are passed as a 10% increase in the syngas production costs) are: *(i)* a 25% reduction of the EPC to 0.76 €/L_{et}, *(ii)* a 98% reduction of the GWP to 1.1 g_{CO2e}/MJ_{et} and, *(iii)* a 70% reduction on the CAC to 435 €/ton_{CO2}. These results bring the fermentation of BBS in line with the fermentation of H_2/CO_2 and suggest that the implementation of this process at industrial scale still depends on the overcoming of technological challenges delivered by the fermentation.

4. Conclusions

The analysis performed led to the acknowledgement that the selection of the gas production process is of paramount importance on the economic and environmental performances of the overall ethanol production process and its potential for replacing fossil-based transportation fuels and for competing with ethanol produced through other renewable pathways.

The fermentation of the steel manufacturing off-gas is the most economically robust process configuration of the three options analyzed over the main current technological limitations of the gas fermentation stage *i.e.*, low tolerance to ethanol, co-production of acetic acid and low mass transfer rates. Such robustness is given by *(i)* the temperature at which the gas is generated, which allows the coverage of all the energy requirements for ethanol distillation, and *(ii)* the low cost assigned to its production, which corresponds to the cost of replacing the energy provided by the BOF off-gas flaring in the steel production process. Moreover, the potential of this process configuration to lead the replacement of fossil-based fuels is constrained by the global throughput of steel and the non-fossil nature of the carbon used for its production.

On the other hand, the fermentation of H_2 produced from the electrolysis of water showed to have the lowest emissions of greenhouse gases, yet at high costs. Such environmental performance is the result of the fact that all energy of this process configuration is derived from low-carbon and renewable wind. In addition, the production of ethanol by this process configuration may improve the energy efficiency of using electricity to power passenger vehicles. The potential for this process configuration to lead the replacement of fossil-based fuels may depend on *(i)* the development of less costly H_2 production technologies, and *(ii)* the development of a microbial strain that tolerates ethanol concentrations above 50 g/L.

The environmental performance of the fermentation of bio-based syngas showed to be the lowest of the three process configurations analyzed. This result may be largely improved by factors external to the fermentation process, if *(i)* bio-syngas was made a utility inside a large industrial complex, where harnessing the advantages of the economy-of-scale, the gas production costs are lowered, *(ii)* if low-carbon and renewable source of energy was used for bio-syngas production and the fermentation process.

Lastly, even the smallest gains in raising the k_La inside the gas fermentor would bring significant benefits on the overall process environmental and economic performances; the same can be argued for the gains on increasing the bacterial tolerance to ethanol.

Declaration of Competing Interest

None.

CRediT authorship contribution statement

Eduardo Almeida Benalcázar: Conceptualization, Methodology, Software, Investigation, Formal analysis, Data curation, Writing – original draft, Writing – review & editing. **Henk Noorman:** Conceptualization, Formal analysis, Writing – review & editing, Supervision, Funding acquisition. **Rubens Maciel Filho:** Conceptualization, Methodology, Writing – review & editing, Funding acquisition. **John A. Posada:** Conceptualization, Methodology, Formal analysis, Writing – review & editing, Supervision.

Acknowledgments

The authors thank DSM and the BE-Basic Foundation for the financial support provided in the form of a PhD scholarship for the author EAB. The authors recognize as well the financial support from the Fundação de Amparo à Persquisa do Estado de São Paulo (FAPESP), Grant 2015/20630-4. This work is part of a Dual Degree PhD project under the agreement between Unicamp and TU Delft.

Supplementary materials

Supplementary material associated with this article can be found, in the online version, at doi:10.1016/j.compchemeng.2022.107670.

References

Abubackar, H.N., Veiga, M.C., Kennes, C., 2015. Carbon monoxide fermentation to ethanol by *Clostridium autoethanogenum* in a bioreactor with no accumulation of acetic acid. Bioresour. Technol. 186, 122–127. doi:10.1016/j.biortech.2015.02.113.

Access Intelligence LLC, 2019. Economic indicators: CEPCI [WWW Document]. Chem. Eng. URL http://www.chemengonline.com/ (accessed 10.24.19).

Achinas, S., Horjus, J., Achinas, V., Euverink, G.J.W., 2019. A PESTLE analysis of biofuels energy industry in Europe. Sustainability 11, 5981. doi:10.3390/su11215981.

Aden, A., Ruth, M., Ibsen, K., Jechura, J., Neeves, K., Sheehan, J., Wallace, B., Montague, L., Slayton, A., Lukas, J., 2002. Lignocellulosic Biomass to Ethanol Process Design and Economics Utilizing Co-Current Dilute Acid Prehydrolysis and Enzymatic Hydrolysis for Corn Stover. National Renewable Energy Laboratory.

Almeida Benalcázar, E., Gevers-Deynoot, B., Noorman, H., Osseweijer, P., Posada, J.A., 2017. Production of bulk chemicals from lignocellulosic biomass via thermochemical conversion and syngas fermentation: a comparative techno-economic and environmental assessment of different site-specific supply chain configurations: techno-economic and environmental assessment of bulk chemicals production though biomass gasification and syngas fermentation. Biofuels Bioprod. Biorefining doi:10.1002/bbb.1790.

Almeida Benalcázar, E., Noorman, H., Maciel Filho, R., Posada, J.A., 2020a. Modeling ethanol production through gas fermentation: a biothermodynamics and mass transfer-based hybrid model for microbial growth in a large-scale bubble column bioreactor. Biotechnol. Biofuels 13, 59. doi:10.1186/s13068-020-01695-y.

Almeida Benalcázar, E., Noorman, H., Maciel Filho, R., Posada, J.A., 2020b. Assessing the sensitivity of technical performance of three ethanol production processes based on the fermentation of steel manufacturing offgas, syngas and a 3:1 mixture between H_2 and CO_2. In: Proceedings of the 30th European Symposium on Computer Aided Process Engineering. Presented at the ESCAPE30. Elsevier, Milano, Italy.

Asimakopoulos, K., Gavala, H.N., Skiadas, I.V., 2018. Reactor systems for syngas fermentation processes: a review. Chem. Eng. J. 348, 732–744. doi:10.1016/j.cej.2018.05.003.

Beneke, D., 2013. Understanding Distillation using Column Profile Maps. Wiley, Hoboken, New Jersey.

Bertsch, J., Müller, V., 2015. Bioenergetic constraints for conversion of syngas to biofuels in acetogenic bacteria. Biotechnol. Biofuels 8. doi:10.1186/s13068-015-0393-x.

Bieda, B., 2012. Life cycle inventory processes of the Arcelor Mittal Poland (AMP) S.A. in Kraków, Poland—basic oxygen furnace steel production: a case study. Int. J. Life Cycle Assess. 17, 463–470. doi:10.1007/s11367-011-0370-y.

Bitnere, K., Searle, S., 2017. Effective Policy Design For Promoting Investment in Advanced Alternative Fuels (White Paper). International Council on Clean Transportation, United States.

B.P. Plc, 2019. BP statistical review of world energy 2019. BP p.l.c, United Kingdom.

Bredwell, M.D., Srivastava, P., Worden, R.M., 1999. Reactor design issues for synthesis-gas fermentations. Biotechnol. Prog. 15, 834–844. doi:10.1021/bp990108m.

Burchart-Korol, D., 2013. Life cycle assessment of steel production in Poland: a case study. J. Clean. Prod. 54, 235–243. doi:10.1016/j.jclepro.2013.04.031.

Burhenne, S., 2013. Monte Carlo based Uncertainty and Sensitivity Analysis for Building Performance Simulation. Karlsruhe Institute of Technology, Aachen (Doctoral thesis).

Caduff, M., Huijbregts, M.A.J., Althaus, H.J., Koehler, A., Hellweg, S., 2012. Wind power electricity: the bigger the turbine, the greener the electricity? Environ. Sci. Technol. 46, 4725–4733. doi:10.1021/es204108n.

Cetinkaya, E., Dincer, I., Naterer, G.F., 2012. Life cycle assessment of various hydrogen production methods. Int. J. Hydrog. Energy 37, 2071–2080. doi:10.1016/j.ijhydene.2011.10.064.

CGEE, 2017. Second-Generation Sugarcane Bioenergy & Biochemicals: Advanced Lowcarbon Fuels for Transport and Industry. Center for Strategic Studies and Management (CGEE), Brasilia.

Ciferno, J., Marano, J., 2002. Benchmarking Biomass Gasification Technologies for Fuels, Chemicals and Hydrogen Production. E2S, United States.

COP-UNFCCC, 2016. Report of the conference of the parties on its 21st session, held in Paris from 30 November to 13 December 2015 : addendum (No. FCCC/CP/2015/10/Add.1).

Daniel, S.L., Hsu, T., Dean, S.I., Drake, H.L., 1990. Characterization of the H_2- and CO-dependent chemolithotrophic potentials of the acetogens *Clostridium thermoaceticum* and *Acetogenium kivui*. J. Bacteriol. 172, 4464–4471. doi:10.1128/jb.172.8.4464-4471.1990.

Davis, L., Scarlata, T., Tan, E., Ross, J., Lukas, J., Sexton, D., 2015. Process design and economics for the conversion of lignocellulosic biomass to hydrocarbons: dilute-acid and enzymatic deconstruction of biomass to sugars and catalytic conversion of sugars to hydrocarbons (Technical report No. NREL/TP-5100-62498). National Renewable Energy Laboratory.

de Medeiros, E.M., Noorman, H., Maciel Filho, R., Posada, J.A., 2020. Production of ethanol fuel via syngas fermentation: optimization of economic performance and energy efficiency. Chem. Eng. Sci. X 5, 100056. doi:10.1016/j.cesx.2020.100056.

de Medeiros, E.M., Posada, J.A., Noorman, H., Filho, R.M., 2019. Dynamic modeling of syngas fermentation in a continuous stirred-tank reactor: multi-response parameter estimation and process optimization. Biotechnol. Bioeng. 116, 2473–2487. doi:10.1002/bit.27108.

Deb, K., 2001. Multi-objective optimization using evolutionary algorithms. Wiley-Interscience Series in Systems and Optimization, 1st ed. John Wiley & Sons, Chichester, New York.

Drake, H.L., Gößner, A.S., Daniel, S.L., 2008. Old acetogens, new light. Ann. N. Y. Acad. Sci. 1125, 100–128. doi:10.1196/annals.1419.016.

Dutta, A., Talmadge, M., Hensley, J., Worley, M., Dudgeon, D., Barton, D., Groenendijk, P., Ferrari, D., Stears, B., Searcy, E., Wright, C., Hess, J., 2011. Process design and economics for conversion of lignocellulosic biomass to ethanol: thermochemical pathway by indirect gasification and mixed alcohol synthesis (Technical report No. NREL/TP-5100-51400). National Renewable Energy Laboratory.

Edenhofer, O., Pichs-Madruga, R., Sokona, Y., Minx, J., Farahani, E., Kadner, S., Seyboth, K., Adler, A., Baum, I., Brunner, S., Eickemeier, P., Kriemann, B., Savolainen, J., Scholmer, S., von Stechow, C., Zwickel, T, 2014. Climate Change 2014: Mitigation of Climate change: Working Group III Contribution to the Fifth Assessment Report of the Intergovernmental Panel On Climate Change. Cambridge University Press, New York, NY.

Efe, Ç., van der Wielen, L.A.M., Straathof, A.J.J., 2005. Technical and Economical Feasibility of Production of Ethanol from Sugar Cane and Sugar Cane Bagasse (B-Basic Internal Report. Delft University of Technology, Delft.

Euro NCAP, 2018. Test results - hyundai NEXO: standard safety equipment. Euro NCAP.

European Parliament, 2018. Directive 2018/2001 of the European Parliament and of the Council of 11 December 2018 on the promotion of the use of energy from renewable sources.

European Parliament, 2009. Directive 2009/28/EC of the European Parliament and of the Council of 23 April 2009 on the promotion of the use of energy from renewable sources and amending and subsequently repealing Directives 2001/77/EC and 2003/30/EC.

Grant, T., Anderson, C., Hooper, B., 2014. Comparative life cycle assessment of potassium carbonate and monoethanolamine solvents for CO_2 capture from post combustion flue gases. Int. J. Greenh. Gas Control 28, 35–44. doi:10.1016/j.ijggc.2014.06.020.

Guo, K., Wang, T., Yang, G., Wang, J., 2017. Distinctly different bubble behaviors in a bubble column with pure liquids and alcohol solutions: distinctly different bubble behaviors in a bubble column. J. Chem. Technol. Biotechnol. 92, 432–441. doi:10.1002/jctb.5022.

Handler, R.M., Shonnard, D.R., Griffing, E.M., Lai, A., Palou-Rivera, I., 2016. Life cycle assessments of ethanol production via gas fermentation: anticipated greenhouse gas emissions for cellulosic and waste gas feedstocks. Ind. Eng. Chem. Res. 55, 3253–3261. doi:10.1021/acs.iecr.5b03215.

Harrison, K., Martin, G., Ramsden, T., Kramer, W., Novachek, F., 2009. The wind-to-hydrogen project: operational experience, performance testing, and systems integration (Technical report No. NREL/TP-550-44082). National Renewable Energy Laboratory.

Heijnen, J.J., Van't Riet, K., 1984. Mass transfer, mixing and heat transfer phenomena in low viscosity bubble column reactors. Chem. Eng. J. 28, B21–B42. doi:10.1016/0300-9467(84)85025-X.

Huang, W.D., Zhang, Y.H.P., 2011. Energy efficiency analysis: biomass-to-wheel efficiency related with biofuels production, fuel distribution, and powertrain systems. PLoS One 6, e22113. doi:10.1371/journal.pone.0022113.

Humbird, D., Davis, S., Tao, L., Kinchin, C., Hsu, D., Aden, A., Schoen, P., Lukas, J., Olthof, B., Worley, M., Sexton, D., Dudgeon, D., 2011. Process design and economics for biochemical conversion of lignocellulosic biomass to ethanol: dilute-acid pretreatment and enzymatic hydrolysis of corn stover (Technical report No. NREL/TP-5100-47764). National Renewable Energy Laboratory, Colorado, USA.

Husebye, J., Brunsvold, A.L., Roussanaly, S., Zhang, X., 2012. Techno economic evaluation of amine based CO_2 capture: impact of CO_2 concentration and steam supply. Energy Procedia 23, 381–390. doi:10.1016/j.egypro.2012.06.053.

IRENA, 2019. Future of Wind: Deployment, Investment, technology, Grid Integration and Socio-Economic Aspects. International Renewable Energy Agency, Abu Dhabi (A Global Energy Transformation paper).

Kechkar, M., Sayed, W., Cabrol, A., Aziza, M., Ahmed Zaid, T., Amrane, A., Djelal, H., 2019. Isolation and identification of yeast strains from sugarcane molasses, dates and figs for ethanol production under conditions simulating algal hydrolysate. Braz. J. Chem. Eng. 36, 157–169. doi:10.1590/0104-6632.20190361s20180114.

Kim, Y.K., Lee, H., 2016. Use of magnetic nanoparticles to enhance bioethanol production in syngas fermentation. Bioresour. Technol. 204, 139–144. doi:10.1016/j.biortech.2016.01.001.

Kundiyana, D.K., Huhnke, R.L., Wilkins, M.R., 2010. Syngas fermentation in a 100-L pilot scale fermentor: design and process considerations. J. Biosci. Bioeng. 109, 492–498. doi:10.1016/j.jbiosc.2009.10.022.

Kurtz, J., Sprik, S., Bradley, T.H., 2019. Review of transportation hydrogen infrastructure performance and reliability. Int. J. Hydrog. Energy 44, 12010–12023. doi:10.1016/j.ijhydene.2019.03.027.

Kwak, T.H., Lee, S., Park, J.W., Maken, S., Yoo, Y.D., Lee, S.H., 2006. Gasification of municipal solid waste in a pilot plant and its impact on environment. Korean J. Chem. Eng. 23, 954–960. doi:10.1007/s11814-006-0014-2.

Ladage, S., Blumenberg, M., Franke, D., Bahr, A., Lutz, R., Schmidt, S., 2021. On the climate benefit of a coal-to-gas shift in Germany's electric power sector. Sci. Rep. 11, 11453. doi:10.1038/s41598-021-90839-7.

Leang, C., Ueki, T., Nevin, K.P., Lovley, D.R., 2013. A genetic system for *Clostridium ljungdahlii*: a chassis for autotrophic production of biocommodities and a model homoacetogen. Appl. Environ. Microbiol. 79, 1102–1109. doi:10.1128/AEM.02891-12.

Lettinga, G., van Velsen, A.F.M., Hobma, S.W., de Zeeuw, W., Klapwijk, A., 1980. Use of the upflow sludge blanket (USB) reactor concept for biological wastewater treatment, especially for anaerobic treatment. Biotechnol. Bioeng. 22, 699–734. doi:10.1002/bit.260220402.

Li, X., 2016. System and method for improved gas dissolution. US 9327251 B2.

Li, X., Cossey, B.J., Trevethick, S.R., 2017. Fermentation of gaseous substrates. US 9,617,509 B2.

Liew, F., Martin, M.E., Tappel, R.C., Heijstra, B.D., Mihalcea, C., Köpke, M., 2016. Gas fermentation - a flexible platform for commercial scale production of low-carbon-fuels and chemicals from waste and renewable feedstocks. Front. Microbiol. 7, 694. doi:10.3389/fmicb.2016.00694.

Majumdar, A., Deutch, J., 2018. Research opportunities for CO_2 utilization and negative emissions at the gigatonne scale. Joule 2, 805–809. doi:10.1016/j.joule.2018.04.018.

Martin, M.E., Richter, H., Saha, S., Angenent, L.T., 2016. Traits of selected *Clostridium* strains for syngas fermentation to ethanol: syngas fermentation strain comparison. Biotechnol. Bioeng. 113, 531–539. doi:10.1002/bit.25827.

Mehmeti, A., Angelis-Dimakis, A., Arampatzis, G., McPhail, S., Ulgiati, S., 2018. Life cycle assessment and water footprint of hydrogen production methods: from conventional to emerging technologies. Environments 5, 24. doi:10.3390/environments5020024.

Millinger, M., Meisel, K., Budzinski, M., Thrän, D., 2018. Relative greenhouse gas abatement cost competitiveness of biofuels in Germany. Energies 11, 615. doi:10.3390/en11030615.

Mock, J., Zheng, Y., Mueller, A.P., Ly, S., Tran, L., Segovia, S., Nagaraju, S., Köpke, M., Dürre, P., Thauer, R.K., 2015. Energy conservation associated with ethanol formation from H_2 and CO_2 in *Clostridium autoethanogenum* involving electron bifurcation. J. Bacteriol. 197, 2965–2980. doi:10.1128/JB.00399-15.

Mohammadi, M., Mohamed, A.R., Najafpour, G.D., Younesi, H., Uzir, M.H., 2014. Kinetic studies on fermentative production of biofuel from ssynthesis gas using *Clostridium ljungdahlii*. Sci. World J. 2014, 1–8. doi:10.1155/2014/910590.

Müller, V., Hess, V., 2017. The minimum biological energy quantum. Front. Microbiol. 8. doi:10.3389/fmicb.2017.02019.

Munasinghe, P.C., Khanal, S.K., 2010. Biomass-derived syngas fermentation into biofuels: opportunities and challenges. Bioresour. Technol. 101, 5013–5022. doi:10.1016/j.biortech.2009.12.098.

Muñoz, I., Flury, K., Jungbluth, N., Rigarlsford, G., i Canals, L.M., King, H., 2014. Life cycle assessment of bio-based ethanol produced from different agricultural feedstocks. Int. J. Life Cycle Assess. 19, 109–119. doi:10.1007/s11367-013-0613-1.

NEDO, 2008. Japanese technologies for energy savings /GHG emissions reduction, global warming countermeasures. New Energy and Industrial Technology Development Organization, Japan.

Noorman, H., 2011. An industrial perspective on bioreactor scale-down: what we can learn from combined large-scale bioprocess and model fluid studies. Biotechnol. J. 6, 934–943. doi:10.1002/biot.201000406.

Oswald, F., Stoll, I.K., Zwick, M., Herbig, S., Sauer, J., Boukis, N., Neumann, A., 2018. Formic acid formation by clostridium Ljungdahlii at elevated pressures of carbon dioxide and hydrogen. Front. Bioeng. Biotechnol. 6. doi:10.3389/fbioe.2018.00006.

Perry, R.H., Green, D.W, 2003. Perry's Chemical Engineers' Handbook, 7th ed. McGraw-Hill, New York internat. ed., [Nachdr.]. ed..

Peters, M.S., Timmerhaus, K.D., 1991. Plant Design and Economics for Chemical Engineers, 4th ed. McGraw-Hill, New York ed, McGraw-Hill chemical Engineering Series.

Phillips, J., Huhnke, R., Atiyeh, H., 2017. Syngas fermentation: a microbial conversion process of gaseous substrates to various products. Fermentation 3, 28. doi:10.3390/fermentation3020028.

Phillips, J.R., Klasson, K.T., Clausen, E.C., Gaddy, J.L., 1993. Biological production of ethanol from coal synthesis gas. Appl. Biochem. Biotechnol. 39/40.

Ragsdale, S.W., Pierce, E., 2008. Acetogenesis and the Wood–Ljungdahl pathway of CO_2 fixation. Biochim. Biophys. Acta BBA Proteins Proteom. 1784, 1873–1898. doi:10.1016/j.bbapap.2008.08.012.

Remus, R., 2013. Best Available Techniques (BAT) Reference Document For Iron and Steel Production Industrial Emissions Directive 2010/75/EU (integrated pollution Prevention and Control). Publications Office of the European Union, Luxembourg.

Rey Porto, M., Carretero, T., Aguado, M., Garde, R., 2010. H_2 production in Sotavento wind farm. In: Proceedings of the WHEC. Presented at the 18th World Hydrogen Energy Conference. WHEC 2010, Essen, Germany.

Richter, H., Martin, M., Angenent, L., 2013. A two-stage continuous fermentation system for conversion of syngas into ethanol. Energies 6, 3987–4000. doi:10.3390/en6083987.

Rochelle, G.T., 2009. Amine scrubbing for CO_2 capture. Science 325, 1652–1654. doi:10.1126/science.1176731.

Sakai, S., Nakashimada, Y., Yoshimoto, H., Watanabe, S., Okada, H., Nishio, N., 2004. Ethanol production from H $_2$ and CO $_2$ by a newly isolated thermophilic bacterium, Moorella sp. HUC22-1. Biotechnol. Lett. 26, 1607–1612. doi:10.1023/B:BILE.0000045661.03366.f2.

Saltelli, A., Ratto, M., Andres, T., Campolongo, F., Cariboni, J., Gatelli, D., Saisana, M., Tarantola, S., 2007. Global Sensitivity Analysis: The Primer. John Wiley & Sons, Ltd, Chichester, UK doi:10.1002/9780470725184.

Sander, R., 2015. Compilation of Henry's law constants (version 4.0) for water as solvent. Atmos. Chem. Phys. 15, 4399–4981. doi:10.5194/acp-15-4399-2015.

Seider, W.D., Seader, J.D., Lewin, D., Widagdo, S, 2010. Product and Process Design Principles: Synthesis, Analysis, and Evaluation, 3rd ed. Wiley, Hoboken, NJ International Student Version. ed..

Shaikh, A., Al-Dahhan, M., 2013. Scale-up of bubble column reactors: a review of current state-of-the-art. Ind. Eng. Chem. Res. 52, 8091–8108. doi:10.1021/ie302080m.

Shen, Y., Brown, R., Wen, Z., 2014a. Syngas fermentation of *Clostridium carboxidivorans* P7 in a hollow fiber membrane biofilm reactor: evaluating the mass transfer coefficient and ethanol production performance. Biochem. Eng. J. 85, 21–29. doi:10.1016/j.bej.2014.01.010.

Shen, Y., Brown, R., Wen, Z., 2014b. Enhancing mass transfer and ethanol production in syngas fermentation of *Clostridium carboxidivorans* P7 through a monolithic biofilm reactor. Appl. Energy 136, 68–76. doi:10.1016/j.apenergy.2014.08.117.

Shen, Y., Brown, R.C., Wen, Z., 2017. Syngas fermentation by *Clostridium carboxidivorans* P7 in a horizontal rotating packed bed biofilm reactor with enhanced ethanol production. Appl. Energy 187, 585–594. doi:10.1016/j.apenergy.2016.11.084.

Simpson, S.D., 2018. CCU-now: fuels and chemicals from waste.

Simpson, S.D., Conrado, R., Mihalcea, C., 2017. Integrated fermentation and electrolysis process. US 2017/0218404 A1.

Simpson, S.D., Fleming, S.E., Havill, A.M., Trevethick, S.R., 2012. Process for producing chemicals using microbial fermentation of substrates comprising carbon monoxide. US 2012/0045807 A1.

Sun, X., Atiyeh, H.K., Huhnke, R.L., Tanner, R.S., 2019. Syngas fermentation process development for production of biofuels and chemicals: a review. Bioresour. Technol. Rep. 7, 100279. doi:10.1016/j.biteb.2019.100279.

Sun, Y., Nozawa, T., Furusaki, S., 1988. Gas holdup and volumetric oxygen transfer coefficient in a three-phase fluidized bed bioreactor. J. Chem. Eng. Jpn. 21, 15–20. doi:10.1252/jcej.21.15.

Teixeira, L.V., Moutinho, L.F., Romão-Dumaresq, A.S., 2018. Gas fermentation of C1 feedstocks: commercialization status and future prospects: commercialization Status of Gas fermentation of C1 feedstocks. Biofuels Bioprod. Biorefining 12, 1103–1117. doi:10.1002/bbb.1912.

The International Consortium for Fire Safety, Health & The Environment, 2011. Safety Issues Regarding Fuel Cell Vehicles and Hydrogen Fueled Vehicles. The International Consortium for Fire Safety, Health & The Environment, Washington DC - USA & Boras - Sweden.

Trevethick, S.R., Bromley, J.C., Waters, G.W., Kopke, M., Tran, L., Jensen, R.O., 2017. Multi-stage bioreactor processes. US 9834792 B2.

Valgepea, K., de Souza Pinto Lemgruber, R., Abdalla, T., Binos, S., Takemori, N., Takemori, A., Tanaka, Y., Tappel, R., Köpke, M., Simpson, S.D., Nielsen, L.K., Marcellin, E., 2018. H_2 drives metabolic rearrangements in gas-fermenting Clostridium autoethanogenum. Biotechnol. Biofuels 11, 55. doi:10.1186/s13068-018-1052-9.

van den Heuvel, J.C., Vredenbregt, L.H.J., Portegies-Zwart, I., Ottengraf, S.P.P., 1995. Acceleration of mass transfer in methane-producing loop reactors. Antonie Van Leeuwenhoek 67, 125–130. doi:10.1007/BF00872200.

van Maris, A.J.A., Konings, W.N., van Dijken, J.P., Pronk, J.T., 2004. Microbial export of lactic and 3-hydroxypropanoic acid: implications for industrial fermentation processes. Metab. Eng. 6, 245–255. doi:10.1016/j.ymben.2004.05.001.

Van't Riet, K., Tramper, J., 1991. Basic Bioreactor Design. M. Dekker, New York.

Vasconcelos, J.M.T., Rodrigues, J.M.L., Orvalho, S.C.P., Alves, S.S., Mendes, R.L., Reis, A., 2003. Effect of contaminants on mass transfer coefficients in bubble column and airlift contactors. Chem. Eng. Sci. 58, 1431–1440. doi:10.1016/S0009-2509(02)00675-9.

Verlaan, P., 1987. Modeling and Characterization of an Airlift-Loop Bioreactor. Wageningen University, Wageningen (PhD Thesis).

World Steel Association, 2019. World Steel in Figures 2019. World Steel Association AISBL, United States.

Yao, J., Kraussler, M., Benedikt, F., Hofbauer, H., 2017. Techno-economic assessment of hydrogen production based on dual fluidized bed biomass steam gasification, biogas steam reforming, and alkaline water electrolysis processes. Energy Convers. Manag. 145, 278–292. doi:10.1016/j.enconman.2017.04.084.

Yasin, M., Jeong, Y., Park, S., Jeong, J., Lee, E.Y., Lovitt, R.W., Kim, B.H., Lee, J., Chang, I.S., 2015. Microbial synthesis gas utilization and ways to resolve kinetic and mass-transfer limitations. Bioresour. Technol. 177, 361–374. doi:10.1016/j.biortech.2014.11.022.

Yusoff, Y., Ngadiman, M.S., Zain, A.M., 2011. Overview of NSGA-II for optimizing machining process parameters. Procedia Eng. 15, 3978–3983. doi:10.1016/j.proeng.2011.08.745.